Numerical Solutions for Boundary Layer Flow of Power-law Nanofluid

By

Fatima Maqbool

A dissertation submitted in partial fulfillment of the requirements
for the degree of Master of Philosophy in Mathematics
Supervised by

Dr. Meraj Mustafa Hashmi

School of Natural Sciences9/3/2014
National University of Sciences and Technology
Islamabad, Pakistan

September 2014

Dedicated

To

My Family

Acknowledgement

In the name of Almighty Allah, Who destined me to do my M. Phil and gave me courage to fulfill this work successfully. This thesis would not have been possible without the support of many individuals, to whom, I owe a great debt of gratitude and would like to sincere thank for their kind support, help and contribution.

First of all, I would like to express my profound gratitude and deep regards to my supervisor Dr. Meraj Mustafa Hashmi for providing precious time, guidance, encouragement and support to accomplish this dissertation. I would like to thank the GEC members Dr. Yousaf Habib (SNS), Dr. Muhammad Asif Farooq (SNS) and Dr. Adnan Maqsood. I extend my gratitude to Sir Ammar Mushtaq (RCMS) for his cooperation and guidence, which helped me in completing this task through various stages.

Finally, I would like to express my heartfelt gratitude and thanks to my family members especially my parents for their constant blessings, prayers and affection. Without their moral support and care it would have been impossible for me to finish this work. May ALMIGHTY give me the enough opportunity to serve for my parents and bestow me on the right path.

Abstract

A numerical study on the MHD stagnation-point flow of electrically conducting power-law nanofluids is presented. The conservation equations are simplified through boundary layer approximations and then reduced to self-similar forms by appropriate substitutions. The recently proposed boundary condition (by A. V. Kuznetsov and D. A. Nield, Int. J. Therm. Sci. 77 (2014) 126-129) is considered which requires nanoparticle volume fraction at the wall to be passively rather than actively controlled. The resulting equations are solved numerically by using fourth-fifth-order Runge- Kutta integration based shooting method. Influence of pertinent parameters on the stream function, temperature and nanoparticle volume fraction is thoroughly investigated. Both integer and non-integer values of power-law index are taken into account. Numerical values showing the trends in wall heat transfer rates have been computed and analyzed. It is seen that penetration depths of thermal and nanoparticle volume fraction boundary layers are decreasing functions of the power-law index. The impact of Brownian motion on the thermal boundary layer is found to be insignificant.

Contents

1	**Introduction**…….	1
1.2	Background of the problem……	1
1.2	Non-Newtonian fluids…….	5
1.3	Boundary layer equations for two-dimensional flow of power-law fluid…….	6
1.4	Boundary layer equations for two-dimensional flow of viscous nanofluid…….	8
1.5	Shooting method for non-linear differential equations……..	9
2	**Numerical Solution for Stagnation-Point Flow of Power-law fluid Past a Stretching Sheet**……...	11
2.1	Introduction……	11
2.2	Mathematical formulation…….	11
	2.2.1 Numerical method ……..…….	14
2.3	Numerical results and discussions ……	14
3	**Boundary Layer Flow of Nanofluid towards a Stretching Sheet**….	18
3.1	Introduction……..	18
3.2	Problem formulation……	18
3.3	Numerical results and discussions ……..….....	20
4	**MHD stagnation-point flow of power-law nanofluid towards a stretching sheet**……	30
4.1	Introduction……	30
4.2	Basic equations……	31
	4.2.1 Numerical method ……..…….	34
4.3	Numerical results and discussions……...	35
5	**Conclusions**……..	43

Chapter 1

Introduction

This chapter includes the recent literature survey of the boundary layer flows over moving or stationary surfaces and boundary layer flows of nanofluids and non-Newtonian fluids. The boundary layer equations for steady two-dimensional flows of power-law fluids and nanofluids are presented. Moreover basic idea of shooting method is described.

1.1 Background of the Problem

The concept of boundary layer was first described by Prandtl [1]. He postulated that flow around a smooth body could be subdivided into two regions: close to the boundaries, in which the fluid viscosity governs the flow, for which the well-known Navier-stokes equations simplify to what we currently refer to as the boundary layer equations. On the other hand, away from the boundaries, viscosity has a small effect and flow is influenced mainly by Euler's potential flow theory. Prandtl [1] showed that within the boundary layer, the Navier-stokes equations can be simplified to a large extent. In contrast to the Navier-stokes equations, which are elliptic type partial differential equation (PDEs), the boundary layer equations have parabolic type behavior that can afford tremendous analytic and computational simplifications. In [1], the boundary layer equations for two-dimensional flow were presented. Some solution approaches of those equations were proposed in this study. In addition, rough calculations of friction drag on flat plate and different aspects of boundary layer separation were given.

The first application of Prandtl's boundary layer concept was presented by Blasius [2]. He considered the laminar boundary layer flow over a flat plate with uniform free

stream velocity. The numerical solution of the Blasius problem was computed by Howarth [3]. Riley [4] studied the flow of an electrically conducting fluid under the influence of magnetic field. In contrast to the Blasius problem the boundary layer flow of an incompressible fluid induced due to a moving flat plate in a quiescent ambient fluid was first described by Sakiadis [5]. In this study, the boundary layer equations for two and three-dimensional flow were provided. Later on Erickson et al [6], discussed the characteristics of heat and mass transfer in the Sakiadis flow for an isothermal porous plate. Tsou et al. [7] investigated the effect of heat transfer on the boundary layer flow due to continuously moving surface with a constant velocity and they experimentally confirmed the numerical results of Sakiadis [5]. Crane [8] considered the flow over a stretching wall and provided exact solution to the Navier-Stokes equation by using a similarity variable technique. Researchers have made various extensions of Crane's problem by studying the influences of body forces due to electromagnetic or gravitational potentials, behavior of porosity or permeability, effects of different wall conditions and non-linear or exponential variation of stretching velocity have been discussed previously. For example, Pavlov [9] analyzed the steady flow of an electrically conducting fluid subjected to magnetic field normal to it. Chakrabarti and Gupta [10] investigated the hydrodynamic flow past a stretching surface with suction or injection. Andersson [11] considered the MHD flow of a viscoelastic fluid over a stretching surface under the influence of magnetic field. He provided the closed form analytic solution of the dimensionless velocity distribution. Ahmad and Mubeen [12] investigated the heat transfer characteristics for large and small Prandtl numbers in a boundary layer flow of an incompressible viscous fluid past a stretching plate with suction. Unsteady three-dimensional flow due to impulsively stretching plate was discussed by Takhar et al. [13]. They solved the formulated differential system by Keller-box method. Heat transfer analysis for flow near a stagnation-point on a stretching sheet was performed by Mahapatra and Gupta [14]. Nazar et al [15] numerically examined the unsteady stagnation-point flow towards a stretching plate. They also computed perturbation solutions valid for small times. Devi and Thiyagarajan [16] considered the stretching sheet in viscous fluid maintained at variable temperature. Radiation and magnetic field effects on the flow of micropolar fluid with variable thermal conductivity were explored by Mahmoud

[17]. Mixed convection flow adjacent to vertical plate was investigated by Ishak et al. [18].

All the above mentioned investigations were confined to flows of Newtonian fluids. However, in view of industrial applications non-Newtonian fluids are more appropriate than the viscous fluids. Some examples of non-Newtonisn fluids include multiphase mixtures, polymer melts and solutions, food products and biological fluids. The laminar boundary layer on a continuous moving flat plate with a constant surface velocity and temperature in a non-Newtonian fluid characterized by a power-law model was studied by Fox et al [19]. They obtained both exact and approximate solutions of the governing mathematical problems. Martison and Pavlov [20] presented a comprehensive discussion on the potential engineering application of non-Newtonian power-law electrically conducting fluids subjected to magnetic field. Chen and Char [21] studied the effect of power-law surface temperature and power-law surface heat flux on the heat transfer due to a linearly stretching sheet. Andersson and Dandapat [22] presented a theoretical study on the flow of power-law fluid due to stretching sheet under the influence of electromagnetic effects. Boundary layer flow of power-law fluid subjected to uniform transverse magnetic field has been addressed by Andersson et al [23]. Cortell [24] presented the numerical study of an electrically conducting power-law fluid over a stretching sheet. Stagnation-point flow of power-law fluid in the presence of transverse magnetic field was numerically explored by Mahapatra et al. [25]. Kumari et al. [26] described the unsteady stagnation-point flow of power-law fluid due to stretching sheet. Mustafa et al. [27] obtained homotopy based series solutions for stagnation-point flow of Casson fluid past a stretching sheet. Steady flow of Maxwell fluid through non-linear Rosseland approximation for thermal radiation is described by Mushtaq et al. [28].

Convective heat transfer in nanofluids has been the subject of great concern for the research community during the last few years. Nanofluid is a liquid suspension formed by dispersing the ultra-fine particles in the base fluids. Researchers have shown that enormous improvement in the heat transfer performance and in particular the solar collection processes is possible through the use of nanofluids [29]. Due to this reason, these are advantageous in enhancing energy efficiency in several areas

including transportation, microelectronics, nuclear reactors, space cooling and power generation. For instance, researchers concluded that optimal utilization of radiation effects due to solar energy is possible through the use of nanofluid based solar collectors. Buongiorno and Hu [30] discussed the heat transfer enhancement via nanoparticles for a nuclear reactor application. Nanofluid's high thermal conductivity may be used for liquid cooling of microchips in computer processors and similar electronic applications. An excellent review study about the convective heat transfer using nanofluids has been presented by Kakaç and Pramuanjaroenkij [31].

Kuznetsov and Nield [32] were probably the first to explore the heat transfer characteristics in a natural convection flow past a vertical plate using Buongiorno's model. Later, Khan and Pop [33] computed numerical solutions for boundary layer flow of nanofluid due to linearly stretching plane surface using implicit finite difference scheme. Homotopy analytic solutions for flow of nanofluid near a stagnation-point past a stretching sheet have been computed by Mustafa et al [34]. Rana and Bhargava [35] obtained finite element solutions for flow of nanofluid due to an extensible sheet stretched with the velocity varying non-linearly with the distance from a fixed point. Combined influence of viscous dissipation and radiation on the boundary layer flow of nanofluid past a prous plate has been described by Motsumi and Makinde [36]. Flow of nanofluid above a non-linearly stretching sheet with linear thermal radiation has reported by Hady et al. [37]. Marangoni convection boundary layer flow has been discussed by Mat et al. [38]. Nadeem et al [39] gave the numerical solution for steady flow of Jeffrey fluid in the presence of nanoparticles. In another paper, Nadeem et al. [40] provided a similar study by considering an Oldroyd-B type fluid. Local similarity solutions for flow of nanofluid over an exponentially stretching sheet were developed by Mustafa et al. [41]. Mustafa et al. [42] solved, both numerically and analytically, the problem of two-dimensional stagnation-point flow of nanofluid past an exponentially stretching sheet. Kandasamy et al. [43] examined the incident radiation effects on steady flow of nanofluid due to solar energy. Unsteady Hiemenz flow of nanofluid across wedge was discussed by Mohamad et al. [44]. Mushtaq et al. [45] recently discussed the nonlinear radiative transfer in the nanofluid flow with an application to solar energy. Exact analytic solutions of unsteady convective heat transfer problem for various nanofluids have

been discussed by Turkyilmazoglu [46]. In another paper, Turkyilmazoglu [47] discussed the heat transfer enhancement via nanoparticles in the flow due to a rotating disk.

1.2 Non-Newtonian fluids

Newton's law of viscosity states that the shear stress is directly proportional to the rate of deformation (shear strain). The fluids which do not follow Newton's law of viscosity are called non-Newtonian fluids. In non-Newtonian fluids, the shear stress is non-linearly proportional to the deformation rate.

For non-Newtonian fluids the power-law model holds. For example, in case of uni-directional flow we have

$$\tau_{yx} \propto \left(\frac{du}{dy}\right)^n \ , n \neq 1 \tag{1.2.1}$$

$$\tau_{yx} = K\left(\frac{du}{dy}\right)^n, \tag{1.2.2}$$

where n is the flow behavior index and K is the consistency index.

Note that the above equation reduces to Newtonian law of viscosity for $n = 1$ and $K = \mu$.

From Eq. (1.2.2)

$$\tau_{yx} = \eta\left(\frac{du}{dy}\right), \tag{1.2.3}$$

where $\eta = K\left(\frac{du}{dy}\right)^{n-1}$ is the apparent viscosity.

Many substances exhibit non-Newtonian behavior including:

- Soap solution and cosmetics
- Food such as butter, jam, cheese, soup, ketchup and yogurt.
- Natural substances such as gums, and vanilla extracts.

- Biological fluids such as semen, blood and saliva.
- Slurries such as cement slurry.

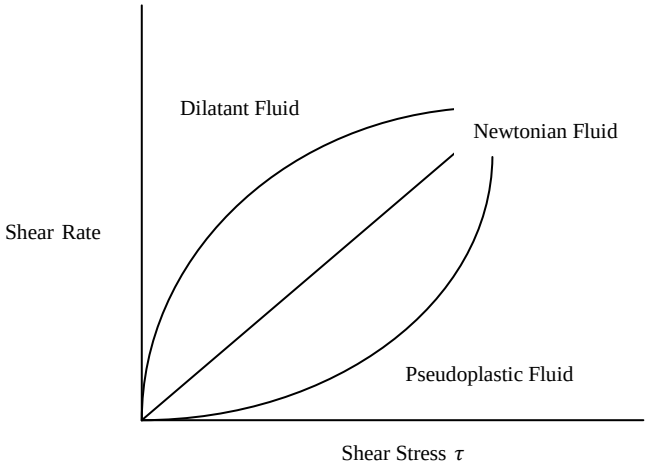

Fig. 1: shows a graphical overview of basic relationship between stress and shear rate of fluids.

1.3 Boundary layer equations for two-dimensional flow of power-law fluid

The constitutive equation is one that expresses the relation between the apparent viscosity or shear stress and the shear rate through the rheological properties of the fluid. Among several non-Newtonian models, the most popular rheological model for non-Newtonian fluid is the power-law or Ostwald-de Waele model. The power-law model provides an adequate representation of many non-Newtonian fluids over the most important range of shear rates. A constitutive relation between the stress tensor τ and the rate of strain tensor D, described by the Ostwald-de Waele power-law model is as under

$$\rho \frac{d\boldsymbol{V}}{dt} = div\tau, \tag{1.3.1}$$

$$\tau \equiv \tau_{ij} = -P\delta_{ij} + 2K\left(2D_{ij}D_{ij}\right)^{\frac{(n-1)}{2}} D_{ij}, \qquad i,j = 1,2,3 \tag{1.3.2}$$

where $\boldsymbol{V}$ is the velocity field, ρ is the fluid density, t is the time, $\frac{d}{dt} = \left(\frac{\partial}{\partial t} + \boldsymbol{V}.\nabla\right)$ is the material time derivative, $\tau \equiv (\tau_{ij})$ is the Cauchy stress tensor, δ_{ij} is the identity tensor, $D_{ij} = \frac{1}{2}\left(\frac{\partial u_i}{\partial x_j} + \frac{\partial u_j}{\partial u_i}\right)$ is the deformation rate tensor, K is the consistency index and n is the flow behavior index.

From Eq. (1.3.2)

$$\tau_{ij} = -P\delta_{ij} + 2K\big(2{D_{11}}^2 + 2{D_{12}}^2 + 2{D_{13}}^2 + 2{D_{21}}^2 + 2{D_{22}}^2 + 2{D_{23}}^2 + 2{D_{31}}^2 + 2{D_{32}}^2 + 2{D_{33}}^2\big)^{\frac{(n-1)}{2}} D_{ij}, \qquad i,j = 1,2,3. \tag{1.3.3}$$

Now using the velocity field for steady two-dimensional flow. i.e. $\boldsymbol{V} = [u(x,y), v(x,y), 0]$, we obtain

$$\tau_{ij} = -P\delta_{ij} + 2K\left(2\left(\frac{\partial u}{\partial x}\right)^2 + \left(\frac{\partial u}{\partial y} + \frac{\partial v}{\partial x}\right)^2 + 2\left(\frac{\partial v}{\partial y}\right)^2\right)^{\frac{(n-1)}{2}} D_{ij},$$

$$i,j = 1,2 \tag{1.3.4}$$

$$\tau_{ij} = -P\delta_{ij} + 2K\left(2\left(\frac{\partial u}{\partial x} + \frac{\partial v}{\partial y}\right)^2 - 4\left(\frac{\partial u}{\partial x}\frac{\partial v}{\partial y}\right) + \left(\frac{\partial u}{\partial y} + \frac{\partial v}{\partial x}\right)^2\right)^{\frac{(n-1)}{2}} D_{ij},$$

$$i,j = 1,2 \tag{1.3.5}$$

Eq.(1.3.5) can be simplified by using the continuity equation as under:

$$\tau_{ij} = -P\delta_{ij} + 2K\left(4\left(\frac{\partial u}{\partial x}\right)^2 + \left(\frac{\partial u}{\partial y} + \frac{\partial v}{\partial x}\right)^2\right)^{\frac{(n-1)}{2}} D_{ij}, \qquad i,j = 1,2 \tag{1.3.6}$$

we now define the Cauchy stress tensor τ as

$$\tau = \begin{bmatrix} \tau_{xx} & \tau_{xy} & \tau_{xz} \\ \tau_{yx} & \tau_{yy} & \tau_{yz} \\ \tau_{zx} & \tau_{zy} & \tau_{zz} \end{bmatrix}. \tag{1.3.7}$$

Using boundary layer approximations

$$u \gg v \quad , \quad \frac{\partial u}{\partial y} \gg \frac{\partial u}{\partial x}, \frac{\partial v}{\partial x}, \frac{\partial v}{\partial y},$$

Eq. (1.3.7) implies

$$\tau_{xy} = \tau_{yx} = k\left(\frac{\partial u}{\partial y}\right)^n \quad , \quad \tau_{xx} = \tau_{yy} = -P. \tag{1.3.8}$$

Using Eq. (1.3.8), the components of momentum Eq. (1.3.1) becomes

$$\rho\left(u\frac{\partial u}{\partial x} + v\frac{\partial u}{\partial y}\right) = \frac{\partial}{\partial x}\tau_{xx} + \frac{\partial}{\partial y}\tau_{xy},$$
$$\rho\left(u\frac{\partial v}{\partial x} + v\frac{\partial v}{\partial y}\right) = \frac{\partial}{\partial x}\tau_{yx} + \frac{\partial}{\partial y}\tau_{yy}, \tag{1.3.9}$$

substituting the values of τ_{xx} and τ_{xy} in Eq. (1.3.9), we get

$$u\frac{\partial u}{\partial x} + v\frac{\partial u}{\partial y} = -\frac{1}{\rho}\frac{\partial P}{\partial x} + \frac{k}{\rho}\frac{\partial}{\partial y}\left(\frac{\partial u}{\partial y}\right)^n, \tag{1.3.12}$$

$$0 = -\frac{\partial P}{\partial y}. \tag{1.3.13}$$

1.4 Boundary layer equations for two-dimensional flow of viscous nanofluid

The mathematical model proposed by Boungiorno [30] accounts for the combined effects of Brownian motion and thermophoretic diffusion of nanoparticles and it was applied by Kuznetsov and Nield [32]. For incompressible flow it is expressed as,

$$\nabla . V = 0, \tag{1.4.1}$$

$$\rho_f\left[\frac{\partial V}{\partial t} + (V.\nabla)V\right] = -\nabla P + \mu\nabla^2 \mathrm{V}, \tag{1.4.2}$$

$$(\rho c)_f \left[\frac{\partial T}{\partial t} + V.\nabla T\right] = k\nabla^2 T + (\rho c)_p \left[D_B \nabla C.\nabla T + \frac{D_T}{T_\infty}(\nabla T.\nabla T)\right], \quad (1.4.3)$$

$$\left[\frac{\partial C}{\partial t} + V.\nabla C\right] = \nabla.\left[D_B \nabla C + D_T \left(\frac{\nabla T}{T_\infty}\right)\right], \quad (1.4.4)$$

where P is the pressure, τ is the stress tensor, C is the nanoparticle volume fraction , T is the nanofluid's temperature, $(\rho c)_p$ is the effective heat capacity of the nanoparticle material, $(\rho c)_f$ is the effective heat capacity of the fluid, D_B is Brownian diffusion coefficient, D_T is thermophoresis diffusion coefficient and the field variables are the velocity $V = V(u, v)$, the Eqs. (1.4.1)-(1.4.4) becomes

$$\frac{\partial u}{\partial x} + \frac{\partial v}{\partial y} = 0, \quad (1.4.5)$$

$$u\frac{\partial u}{\partial x} + v\frac{\partial u}{\partial y} = -\frac{1}{\rho_f}\frac{\partial p}{\partial x} + \nu\left(\frac{\partial^2 u}{\partial x^2} + \frac{\partial^2 u}{\partial y^2}\right), \quad (1.4.6)$$

$$u\frac{\partial v}{\partial x} + v\frac{\partial v}{\partial y} = -\frac{1}{\rho_f}\frac{\partial p}{\partial y} + \nu\left(\frac{\partial^2 v}{\partial x^2} + \frac{\partial^2 v}{\partial y^2}\right), \quad (1.4.7)$$

$$u\frac{\partial T}{\partial x} + v\frac{\partial T}{\partial y} = \alpha\left(\frac{\partial^2 T}{\partial x^2} + \frac{\partial^2 T}{\partial y^2}\right) + \tau\left\{D_B\left(\frac{\partial C \partial T}{\partial x \partial x} + \frac{\partial C \partial T}{\partial y \partial y}\right) + \left(\frac{D_T}{T_\infty}\right)\left[\left(\frac{\partial T}{\partial x}\right)^2 + \left(\frac{\partial T}{\partial y}\right)^2\right]\right\}, \quad (1.4.8)$$

$$u\frac{\partial C}{\partial x} + v\frac{\partial C}{\partial y} = D_B\left(\frac{\partial^2 C}{\partial x^2} + \frac{\partial^2 C}{\partial y^2}\right) + \left(\frac{D_T}{T_\infty}\right). \quad (1.4.9)$$

1.5 Shooting method for non-linear differential equation

The shooting method is used for solving boundary value problem by reducing it to the solution of an initial value problem. Consider the second order ODE

$$y'' = f(x, y, y'), \quad a \le x \le b, \quad (1.5.1)$$

with the following boundary conditions

$$y(a) = c_1, \quad y(b) = c_2. \tag{1.5.2}$$

The first step is to reduce differential equation system into first order as,

$$y' = p, \qquad p' = r, \tag{1.5.1}$$

with

$$y(a) = c_1, \quad y'(a) = q, \tag{1.5.2}$$

where q is to be determined such that the boundary condition at $x = b$ is satisfied.

$$\lim_{t\to\infty} y(b, q_t) = y(b)c_2. \tag{1.5.3}$$

Generate a sequence $q_1, q_2, \ldots$ with q_0 as the initial guess and the condition is that the iteration must stop when

$$y(b, q) - c_2 = 0, \tag{1.5.4}$$

it is a non-linear equation in q(variable).

The above first order ODEs along with initial conditions (1.5.2) are solved by standard fourth-order Runge-Kutta integration technique. Consider a Newton-Raphson method to generate a sequence q_t.

q_0 is the initial guess and generate the remaining terms by using

$$q_t = q_{t-1} - \frac{(y(b, s_{t-1}) - c_2)}{\frac{dy}{dq}(b, s_{t-1})}. \tag{1.5.5}$$

Newton-Raphson formula for two or more variables is defined as

$$q_t = q_{t-1} - \frac{(y(b, s_{t-1}) - c_2)}{|J|}, \tag{1.5.6}$$

where J is the Jacobian matrix.

Chapter 2

Numerical solution for stagnation-point flow of power-law fluid past a stretching sheet

This chapter is arranged in the following manner.

Section 2.1 contains the introduction. Section 2.2 includes the mathematical formulation of the problem. Numerical solution with the help of shooting method is described in section 2.3. Numerical results are presented and discussed in section 2.4.

2.1 Introduction

This chapter is a review work of Mahapatra et al [25]. It describes the steady, two-dimensional stagnation-point flow of an electrically conducting power-law fluid towards a stretching surface in the presence of a transverse magnetic field. The equations are first modeled and then solved numerically by shooting method. Results for dimensionless velocity and wall shear stress are presented and discussed.

2.2 Mathematical formulation

We consider the two dimensional flow of power-law fluid near a stagnation-point towards a stretching sheet. This sheet is coincident with the x-axis and the fluid occupies the region $y \geq 0$. The sheet is stretched in its own plane through the application of two equal and opposite forces while keeping the origin fixed. Let $U_w(x) = cx$ be the velocity of the stretching sheet and $U(x) = ax$ is the velocity outside the boundary layer with $c, a > 0$ are constants. The flow is subjected to transverse magnetic field of strength B_0 in the vertical direction. Using the velocity

field $\boldsymbol{V} = [u(x,y), v(x,y), 0]$ the boundary layer equations governing the two-dimensional stagnation-point flow of power-law fluid can be written as

$$\frac{\partial u}{\partial x} + \frac{\partial v}{\partial y} = 0, \tag{2.2.1}$$

$$u\frac{\partial u}{\partial x} + v\frac{\partial u}{\partial y} = U\frac{dU}{dx} + \frac{1}{\rho}\frac{\partial \tau_{xy}}{\partial y} - \frac{\sigma {B_0}^2}{\rho}(u - U), \tag{2.2.2}$$

where u and v are the velocity components along the x- and y- directions respectively, ρ is density, σ is the electrical conductivity, B_0 is magnetic field and τ_{xy} is shear stress. It can be seen through the geometry of the problem that $\partial u/\partial y < 0$ when $a/c < 1$ and $\partial u/\partial y > 0$ when $a/c > 1$.

$$\tau_{xy} = -K\left(-\frac{\partial u}{\partial y}\right)^n, \tag{2.2.3}$$

substituting the expression for τ_{yx} in both cases, we obtain,

$$u\frac{\partial u}{\partial x} + v\frac{\partial u}{\partial y} = U\frac{dU}{dx} - \frac{K}{\rho}\frac{\partial}{\partial y}\left(-\frac{\partial u}{\partial y}\right)^n - \frac{\sigma {B_0}^2}{\rho}(u - U), \tag{2.2.4}$$

$$u\frac{\partial u}{\partial x} + v\frac{\partial u}{\partial y} = U\frac{dU}{dx} + \frac{K}{\rho}\frac{\partial}{\partial y}\left(\frac{\partial u}{\partial y}\right)^n - \frac{\sigma {B_0}^2}{\rho}(u - U), \tag{2.2.5}$$

with the boundary conditions

$$\begin{gathered} u = cx, v = 0 \quad \text{at} \quad y = 0, \\ u = U(x) = ax, \;\; v = -ay \;\; \text{as} \;\; y \to \infty, \end{gathered} \tag{2.2.6}$$

using the following dimensionless variables,

$$\psi = \left(\frac{K/\rho}{c^{1-2n}}\right)^{\frac{1}{n+1}} x^{\frac{2n}{n+1}} f(\eta) \quad , \quad \eta = y\left(\frac{c^{2-n}}{K/\rho}\right)^{1/(n+1)} x^{(1-n)/(1+n)}, \tag{2.2.7}$$

we obtain

$$u = cxf' \ , \ \frac{\partial u}{\partial x} = cf' \ , \ \frac{\partial u}{\partial y} = cx^{\frac{2}{1+n}}\left(\frac{c^{2-n}}{K/\rho}\right)^{\frac{1}{n+1}} f'',$$

$$U = ax \ , \ \frac{dU}{dx} = a \ , \ v = -\left(\frac{K/\rho}{c^{1-2n}}\right)^{\frac{1}{n+1}}\left(\frac{2n}{n+1}\right)x^{\frac{n-1}{n+1}}f, \tag{2.2.8}$$

the continuity Eq. (2.2.1) is satisfied and momentum equations (2.2.4) and (2.2.5) takes the following form

$$c^2xf'^2 - c^2x\left(\frac{2n}{n+1}\right)ff'' = a^2x + \frac{K}{\rho}\left\{nc^n x^{\frac{2n}{n+1}}\left(\frac{c^{2-n}}{K/\rho}\right)^{\frac{n}{n+1}}(-f'')^{n-1}f'''\right\}$$

$$\left\{\left(\frac{c^{2-n}}{K/\rho}\right)^{1/(n+1)} x^{(1-n)/(1+n)}\right\} - \frac{\sigma {B_0}^2}{\rho}x(cf' - a), \tag{2.2.9}$$

$$c^2xf'^2 - c^2x\left(\frac{2n}{n+1}\right)ff'' = a^2x + \frac{K}{\rho}\left\{nc^n x^{\frac{2n}{n+1}}\left(\frac{c^{2-n}}{K/\rho}\right)^{\frac{n}{n+1}}(f'')^{n-1}f'''\right\}$$

$$\left\{\left(\frac{c^{2-n}}{K/\rho}\right)^{1/(n+1)} x^{(1-n)/(1+n)}\right\} - \frac{\sigma {B_0}^2}{\rho}x(cf' - a), \tag{2.9.10}$$

simplifying and then combining the above equations, one obtains

$$c^2xf'^2 - c^2x\left(\frac{2n}{n+1}\right)ff'' = a^2x + nxc^2\left[sgn\left(\frac{a}{c} - 1\right)f''\right]^{n-1}f'''$$

$$-\frac{\sigma {B_0}^2}{\rho}x(cf' - a), \tag{2.2.11}$$

dividing by c^2x, we get

$$n[sgn(\lambda - 1)f'']^{n-1}f''' + \left(\frac{2n}{n+1}\right)ff'' - f'^2 - Mf' + M\lambda + \lambda^2 = 0, \tag{2.2.12}$$

where $M = \sigma {B_0}^2/c\rho$ is the magnetic parameter and $\lambda = a/c$ is the velocity ratio. The dimensionless boundary conditions through (2.2.7) can be written as

$$f(0) = 0,\ f'(0) = 1,\ f'(\infty) = \lambda. \qquad (2.2.13)$$

Using Eq. (2.2.7), the skin friction coefficient $c_f = \tau_{yx}\big|_{y=0}/(1/2)\rho {U_w}^2$ becomes

$$Re_x^{1/(1+n)} C_f = 2[sgn(\lambda - 1)f''(0)]^n.$$

2.2.1 Numerical method

The transformed momentum Eqs. (2.2.12) subject to the boundary conditions are solved numerically for different values of λ, magnetic parameter M and the power-law index n. Eq. (2.2.12) can be written as a system of three first-order differential equations by substituting $x_1 = \eta,\ x_2 = f,\ x_3 = f',\ x_4 = f''$. We obtain

$$\begin{pmatrix} x_1' \\ x_2' \\ x_3' \\ x_4' \end{pmatrix} = \begin{pmatrix} 1 \\ x_3 \\ x_4 \\ \dfrac{-\left(\frac{2n}{n+1}\right) x_2 x_4 + {x_3}^2 + M x_3 - M\lambda - \lambda^2}{n[sgn(\lambda - 1)x_4]^{n-1}} \end{pmatrix},$$

and the corresponding initial conditions are

$$\begin{pmatrix} x_1(0) \\ x_2(0) \\ x_3(0) \\ x_4(0) \end{pmatrix} = \begin{pmatrix} 0 \\ 0 \\ 1 \\ u_1 \end{pmatrix}.$$

The above nonlinear ODEs along with initial conditions are solved by standard fourth-order Runge-Kutta integration technique. Suitable value of the unknown initial condition u_1 is approximated and optimized through Newton's method until the boundary conditions at infinity $f'(\infty) = \lambda$ is satisfied with the error less than 10^{-7}. The computations have been performed by using MATLAB.

2.3 Numerical results and discussion

To examine the physical effects of the embedded parameters, we have plotted Figs. 2.1 and 2.2 and prepared tables $2.1 - 2.4$. These tables indicate that shear stress at the

wall decreases with an increase in n when $\lambda < 1$. However it is an increasing function of n when $\lambda > 1$. Moreover variation in $f''(0)$ with n is non-monotonic when ratio of free stream velocity to the velocity of stretching sheet largely differs from one. Fig. 2.1 represents the variation in x-component of velocity with M and λ for pseudoplastic fluid ($n = 0.4$). It is clear that velocity parallel to the stretching surface decreases with increasing values of magnetic parameter M when $\lambda < 1$ however it is increases with increase in M when $\lambda > 1$. Irrespective of chosen value of λ the profiles tends to λ faster when M is increased indicating a decrease in the momentum boundary layer. This decrease in the momentum transport is the consequence of resistance offered by the Lorentz force normal to the flow. Fig. 2.2 shows the velocity profiles corresponding to the data considered in Fig. 2.1 in the case of dilatant fluid fluid ($n = 2.0$). It can be concluded that behaviors of parameters in the case of pseudoplastic and dilatants fluids on the boundary layer are only quantitative. However the momentum boundary layer is thicker in the case of pseudoplastic fluids when compared with the dilatants fluids.

Table 2.1: Variation of $-f''(0)$ with n and M when $\lambda = 0.2$.

n \ M	0.0	0.5	1.0	1.5	2.0
0.6	1.0018	1.2506	1.4725	1.6757	1.8651
0.8	0.9424	1.1356	1.3058	1.4600	1.6021
1.0	0.9181	1.0768	1.2156	1.3404	1.4546
1.5	0.9066	1.0170	1.1127	1.1978	1.2749
2.0	0.9133	0.9983	1.0715	1.1363	1.1946

Table 2.2: Variation of $-f''(0)$ with n and M when $\lambda = 0.9$.

n \ M	0.0	0.5	1.0	1.5	2.0
0.6	0.1104	0.1253	0.1393	0.1525	0.1650
0.8	0.1314	0.1464	0.1603	0.1734	0.1857
1.0	0.1547	0.1699	0.1839	0.1969	0.2092
1.5	0.2155	0.2309	0.2451	0.2581	0.2703
2.0	0.3272	0.3422	0.3559	0.3683	0.3798

Table 2.3: Variation of $f''(0)$ with n and M when $\lambda = 1.1$.

n \ M	0.0	0.5	1.0	1.5	2.0
0.6	0.1193	0.1337	0.1471	0.1599	0.1721
0.8	0.1407	0.1549	0.1683	0.1808	0.1927
1.0	0.1643	0.1787	0.1920	0.2045	0.2163
1.5	0.2257	0.2402	0.2536	0.2660	0.2777
2.0	0.2844	0.2988	0.3119	0.3241	0.3355

Table 2.4: Variation of $f''(0)$ with n and M when $\lambda = 1.5$.

n \ M	0.0	0.5	1.0	1.5	2.0
0.6	1.0174	1.1169	1.2114	1.3019	1.3887
0.8	0.9434	1.0218	1.0958	1.1661	1.2333
1.0	0.9095	0.9750	1.0364	1.0946	1.1499
1.5	0.8853	0.9325	0.9765	1.0178	1.0568
2.0	0.8871	0.9244	0.9591	0.9914	1.0218

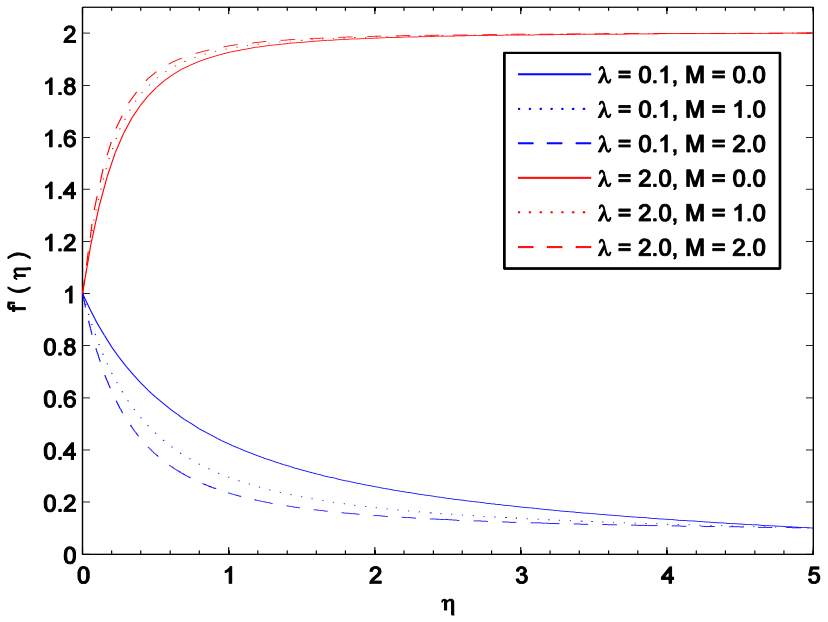

Fig. 2.1: Influence of λ and M on velocity profile when $n = 0.4$ (Pseudoplastic fluid).

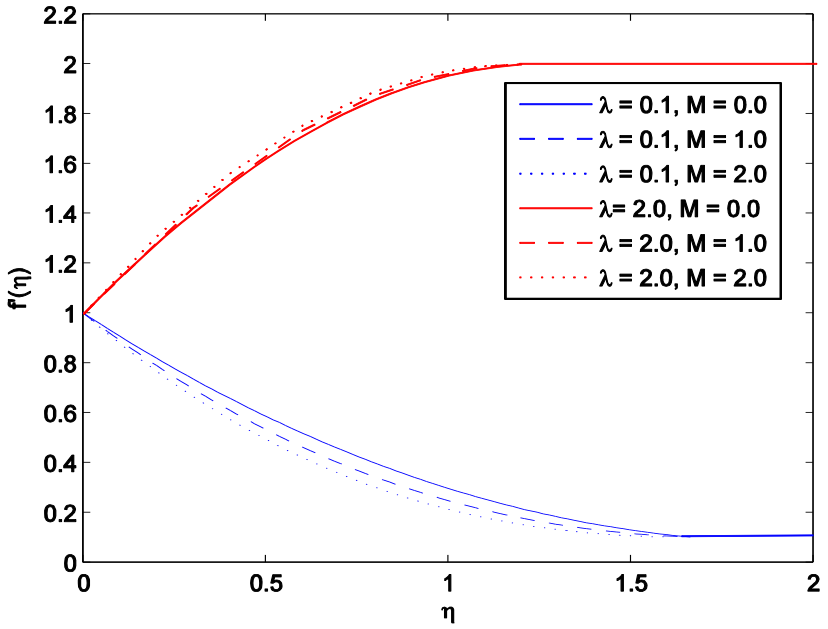

Fig. 2.2: Influence of λ and M on velocity profile when $n = 2.0$ (Dilatant fluid).

Chapter 3

Boundary layer flow of nanofluid towards a stretching sheet

Section 3.1 contains the introduction. Mathematical model and boundary layer equations for two-dimensionl flow of nanofluid are presented in section 3.2. The numerical results are presented and discussed in section 3.3.

3.1 Introduction

This chapter is a review work of Khan and Pop [33]. It deals with the boundary-layer flow of viscous nanofluid due to linearly stretching sheet. Boundary layer equations governing the conservation of mass, momentum, energy and nanoparticles are obtained using Boungiorno's model [30] and then reduced into self-similar forms using similarity transformations. A numerical solution is developed which depends on the Prandtl number Pr, Lewis number Le, Brownian motion number Nb and thermophoresis number Nt. The resulting differential equations have been solved numerically by shooting method and by the built-in function bvp4c of MATLAB.

3.2 Problem formulation

Consider the incompressible flow of nanofluid due to a linearly stretching sheet. The sheet is stretched with the velocity $u_w(x) = ax$, where a is a constant and x is the coordinate considered along the stretching surface. The fluid occupies the region $y \geq 0$. The sheet is maintained at constant temperature T_w and nanoparticle volume fraction at the sheet is assumed to be C_w. Ambient temperature and nanoparticle volume fraction are denoted by T_∞ and C_∞ respectively. Using the velocity field $\boldsymbol{V} = [u(x,y),\ v(x,y), 0]$ (in the mathematical model given by Kuznetsov and Nield

[32]) and applying the usual boundary layer assumptions, we obtain the following set of equations:

$$\frac{\partial u}{\partial x}+\frac{\partial v}{\partial y}=0, \tag{3.2.1}$$

$$u\frac{\partial u}{\partial x}+v\frac{\partial u}{\partial y}=-\frac{1}{\rho_f}\frac{\partial p}{\partial x}+\nu\left(\frac{\partial^2 u}{\partial y^2}\right), \tag{3.2.2}$$

$$u\frac{\partial T}{\partial x}+v\frac{\partial T}{\partial y}=\alpha\left(\frac{\partial^2 T}{\partial y^2}\right)+\tau\left\{D_B\left(\frac{\partial C\partial T}{\partial y\partial y}\right)+\left(\frac{D_T}{T_\infty}\right)\left(\frac{\partial T}{\partial y}\right)^2\right\}, \tag{3.2.3}$$

$$u\frac{\partial C}{\partial x}+v\frac{\partial C}{\partial y}=D_B\left(\frac{\partial^2 C}{\partial y^2}\right)+\left(\frac{D_T}{T_\infty}\right)\left(\frac{\partial^2 T}{\partial y^2}\right), \tag{3.2.4}$$

boundary conditions are

$$\begin{gathered} u=u_w(x)=ax,\quad v=0,\quad T=T_w,\quad C=C_w \text{ at } y=0,\\ u=0,\quad T\to T_\infty,\quad C\to C_\infty \text{ as } y\to\infty. \end{gathered} \tag{3.2.5}$$

Where p is the fluid pressure, ρ_f is the density of base fluid, α is thermal diffusivity, ν is the kinematic viscosity, a is a positive constant, D_B is the Brownian diffusion coefficient, D_T is the thermophoretic diffusion coefficient and $\tau=(\rho c)_p/(\rho c)_f$ is the ratio between the effective heat capacity of the Nanoparticle material and heat capacity of the fluid.

Using these following dimensionless variables

$$\psi=\sqrt{a\nu}xf(\eta),\qquad \eta=\sqrt{\frac{a}{\nu}}y,\qquad \theta(\eta)=\frac{T-T_\infty}{T_w-T_\infty},\qquad \phi(\eta)=\frac{C-C_\infty}{C_w-C_\infty}, \tag{3.2.6}$$

using the dimensionless variables from Eq. (3.2.6), we get

$$u=axf'(\eta), v=-\sqrt{\nu a}f(\eta), \frac{\partial u}{\partial x}=af', \frac{\partial^2 u}{\partial x^2}=0, \frac{\partial u}{\partial y}=ax\sqrt{\frac{a}{\nu}}f'', \tag{3.2.7}$$

$$\frac{\partial^2 u}{\partial y^2} = \frac{a^2 x}{\nu} f''', \frac{\partial T}{\partial x} = 0, \frac{\partial^2 T}{\partial x^2} = 0, \frac{\partial T}{\partial y} = \sqrt{\frac{a}{\nu}}(T_w - T_\infty)\theta',$$

$$\frac{\partial^2 T}{\partial y^2} = \frac{a}{\nu}(T_w - T_\infty)\theta'', \frac{\partial C}{\partial x} = 0, \frac{\partial^2 C}{\partial x^2} = 0, \frac{\partial C}{\partial y} = (C_w - C_\infty)\sqrt{\frac{a}{\nu}}\phi',$$

$$\frac{\partial^2 C}{\partial y^2} = \frac{a}{\nu}(C_w - C_\infty)\phi'',$$

inserting Eq. (3.2.7) in Eq. (3.2.2)-(3.2.4), we obtain

$$f''' + ff'' - f'^2 = 0, \tag{3.2.8}$$

$$\theta'' + Prf\theta' + PrNb\theta'\phi' + PrNt\theta'^2 = 0, \tag{3.2.9}$$

$$\phi'' + Lef\phi' + \frac{Nt}{Nb}\theta'' = 0, \tag{3.2.10}$$

and the boundary conditions (3.2.5) become

$$f(0) = 0, \quad f'(0) = 1, \quad \theta(0) = 1, \quad \phi(0) = 1,$$
$$f'(\infty) = 0, \quad \theta(\infty) = 0, \quad \phi(\infty) = 0. \tag{3.2.11}$$

The quantities of practical interest are the local Nusselt number and local Sherwood number defined as under:

$$Nu = \frac{xq_w}{k(T_w - T_\infty)} \quad , \quad Sh = \frac{xq_m}{k(C_w - C_\infty)}, \tag{3.2.12}$$

where $q_w = -k\left(\partial T/\partial y\right)\Big|_{y=0}$ are the wall heat flux and $q_m = -D_B\left(\partial C/\partial y\right)\Big|_{y=0}$ wall mass flux. Eq. (3.2.12) in non-dimensional form $Re_x^{-1/2} Nu = -\theta'(0)$, $Re_x^{-1/2} Sh = -\phi'(0)$ where $Re_x = u_w(x)\, x/\nu$ is the local Renolds number.

3.3 Numerical results and discussion

The numerical solution of governing differential system Eq. (3.2.8)-(3.2.10) subjected to the boundary conditions (3.2.11) is obtained by shooting method with fourth order Runge-kutta integration technique. For this purpose, we first reduce the equations (3.2.8)-(3.2.10) into the first order system and the conditions (3.2.11) as under

$$\begin{pmatrix} x_1' \\ x_2' \\ x_3' \\ x_4' \\ x_5' \\ x_6' \\ x_7' \\ x_8' \end{pmatrix} = \begin{pmatrix} 1 \\ x_3 \\ x_4 \\ \dfrac{-\left(\frac{2n}{n+1}\right)x_2x_4 + {x_3}^2 + Mx_3 - M\lambda - \lambda^2}{n[sgn(\lambda-1)x_4]^{n-1}} \\ x_6 \\ -\left(\dfrac{2n}{n+1}\right)Prx_2x_6 + Nbx_8x_6 + Ntx_6{}^2 \\ x_8 \\ -\left(\dfrac{2n}{n+1}\right)Lex_2x_8 - \dfrac{Nt}{Nb}x_6' \end{pmatrix},$$

$$\begin{pmatrix} x_1(0) \\ x_2(0) \\ x_3(0) \\ x_4(0) \\ x_5(0) \\ x_6(0) \\ x_7(0) \\ x_8(0) \end{pmatrix} = \begin{pmatrix} 0 \\ 0 \\ 1 \\ u_1 \\ 1 \\ u_2 \\ 1 \\ u_3 \end{pmatrix}.$$

Suitable values of missing slopes $f''(0)$, $\theta'(0)$ and $\phi'(0)$ are guessed and then the integration is carried out. Finally successive iterations are performed using Newton's method until the boundary condition at sufficiently large value of η is satisfied.

Table 3.1 shows the comparison of our results with Khan and Pop [33] for reduced Nusselt number $-\theta'(0)$ when the effects of Nt and Nb are neglected. The heat transfer rate increases with an increase in the Prandtl number Pr. The variation of the reduced Nusselt number Nur and Sherwood number Shr with Nb and Nt for $Pr = 10$ and $Le = 10$ is presented in tables 3.2 and 3.3. The heat transfer rate decreases with an increase in Brownian motion and thermophoresis parameters. However the reduced sherwood number increases when Nb and Nt are increased.

Table 3.1: Comparison of results for dimensionless heat transfer rate $-\theta'(0)$ for different values of Pr when $Nt = Nb = 10^{-5}$.

Pr	$-\theta'(0)$		
	Khan and Pop[39]	Shooting method	bvp4c
0.07	0.0663	0.0663	0.0663
0.20	0.1691	0.1691	0.1691
0.70	0.4539	0.4539	0.4539
2.00	0.9113	0.9113	0.9113
7.00	1.8954	1.8954	1.8954
20.00	3.3539	3.3539	3.3539
70.00	6.4621	6.4621	6.4621

Table 3.2: Variation of dimensionless heat transfer rate $-\theta'(0)$ for different values of Nt and Nb when $Pr = 10$ and $Le = 10$.

Nt \ Nb	0.1	0.2	0.3	0.4	0.5
0.1	0.9524	0.5056	0.2522	0.1194	0.0543
0.2	0.6932	0.3654	0.1816	0.0859	0.0390
0.3	0.5201	0.2731	0.1355	0.0641	0.0291
0.4	0.4026	0.2110	0.1046	0.0495	0.0225
0.5	0.3211	0.1681	0.0833	0.0394	0.0179

Table 3.3: Variation of dimensionless mass transfer rate $-\phi'(0)$ for different values of Nt and Nb when $Pr = 10$ and $Le = 10$.

Nt \ Nb	0.1	0.2	0.3	0.4	0.5
0.1	2.1294	2.3819	2.4100	2.3997	2.3836
0.2	2.2740	2.5152	2.5150	2.4807	2.4468
0.3	2.5286	2.6555	2.6088	2.5486	2.4984
0.4	2.7952	2.7818	2.6876	2.6038	2.5399
0.5	3.0351	2.8883	2.7519	2.6483	2.5731

The effects of Brownian motion and thermophoretic diffusion on the temperature is presented in Fig. 3.1. It is found that temperature decreases with increasing values of Nt and Nb. The dimensionless heat transfer rate versus Nt is plotted for different values of Nb in Fig. 3.2. Plots are shown for $Pr = 1$ and $Pr = 10$. It is found that dimensionless heat transfer rate decreases with an increase in Nb and Nt. The wall heat transfer rate is largely influenced with the variation of parameters at large Le say ($Le = 25$) when compared with smaller values of Le (say $Le = 5$).

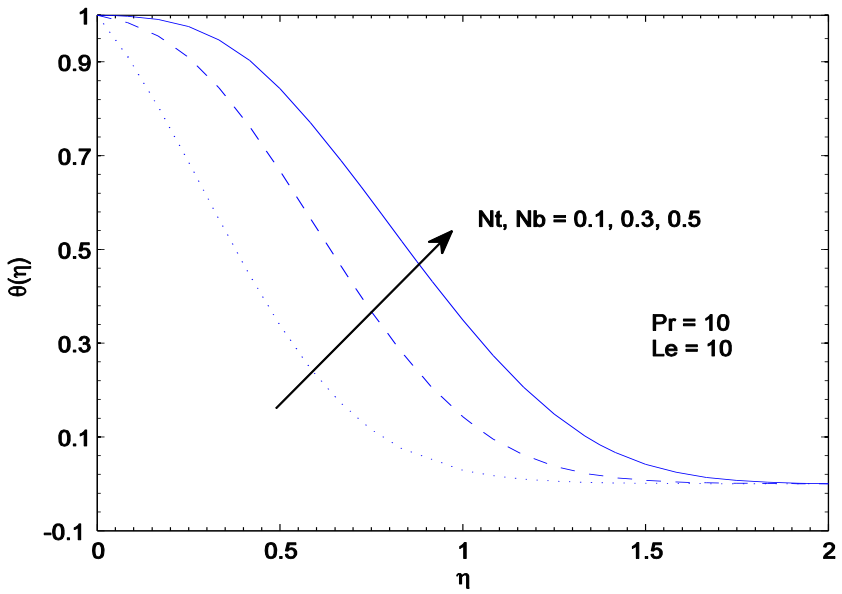

Fig. 3.1: Influence of Nt and Nb on temperature distribution.

(a)

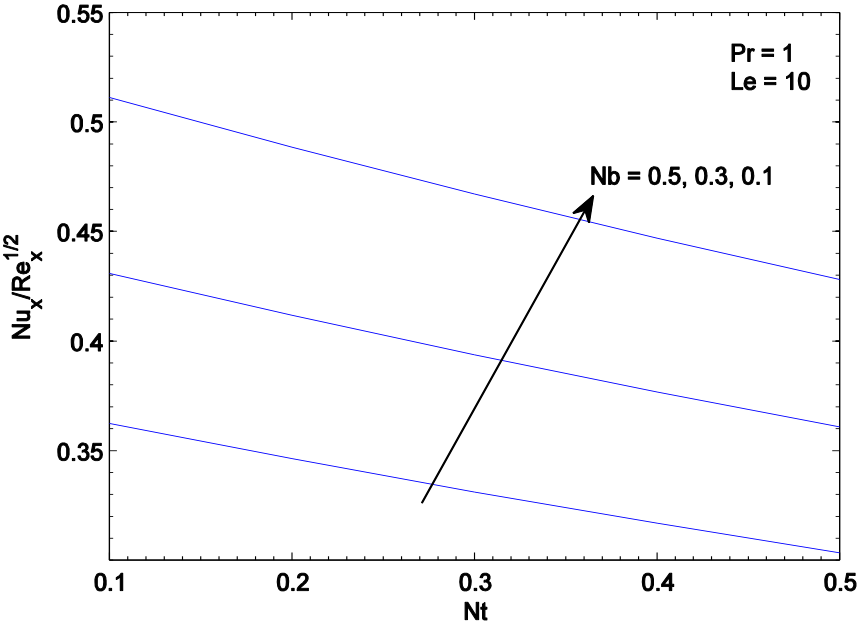

(b)

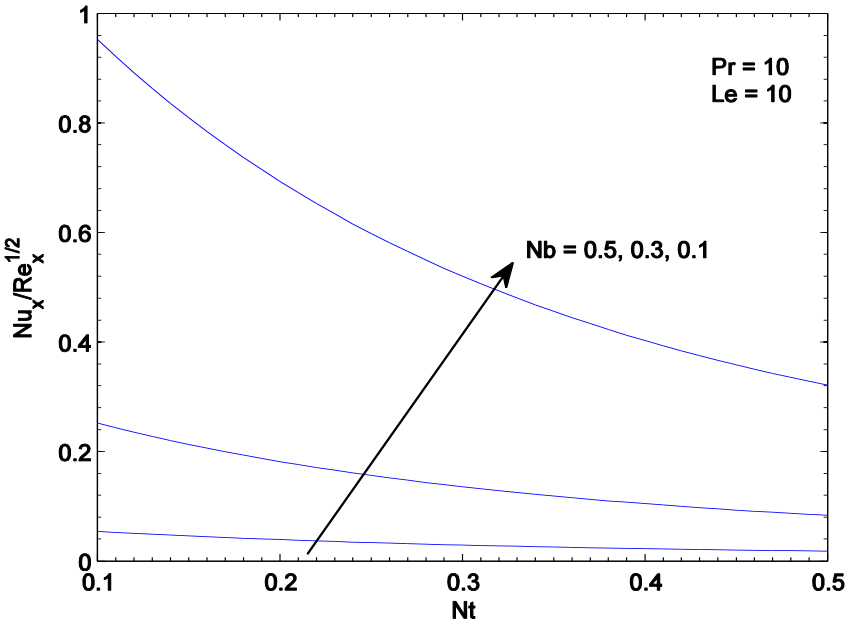

Fig. 3.2: Influence of Nb and Pr on dimensionless heat transfer rates.

(a)

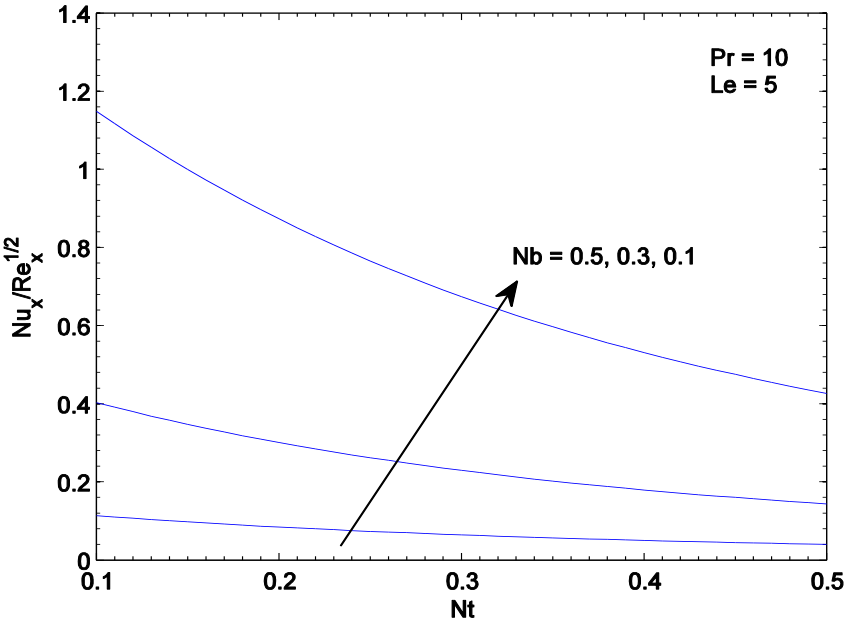

(b)

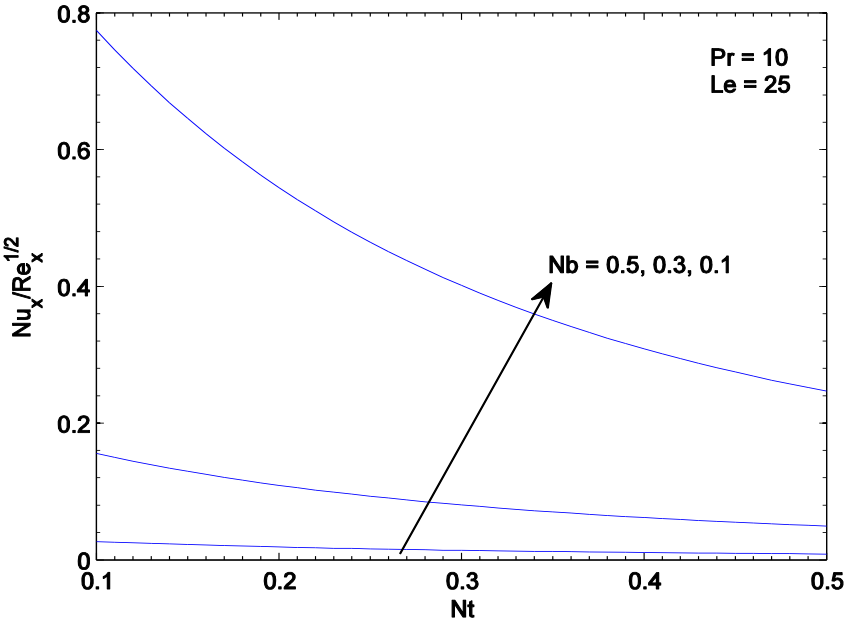

Fig. 3.3: Influence of Nb and Le on dimensionless heat transfer rates.

Fig. 3.4 illustrates the outcome of an increase in the Brownian motion parameter Nb on the nanoparticles volume fraction ϕ. We observe that ϕ increases by decreasing Nb. Fig. 3.5 is plotted to analyze the effects of Lewis number Le on ϕ. It is found that ϕ decreases as the Lewis number Le. This is because increasing values of Le meets with the smaller mass diffusion and hence offers less penetration depth for nanoparticles volume fraction boundary layer. Fig. 3.6 and 3.7 show the variation in dimensionless mass transfer rates versus Nt for specified values of other parameters. It is clear from Fig. 3.6 that the dimensionless mass transfer rate decreases with the increase in Nt for small Pr. However, for large values of Pr, the dimensionless mass transfer rate increases with decrease in Nb and increase in Nt. The influence of Le on the nanoparticles volume fraction profile is shown in Fig. 3.7 for the same values of Pr. The change in dimensionless mass transfer rates is found to be higher for smaller values of Nb and this change increases with the increase in Nt.

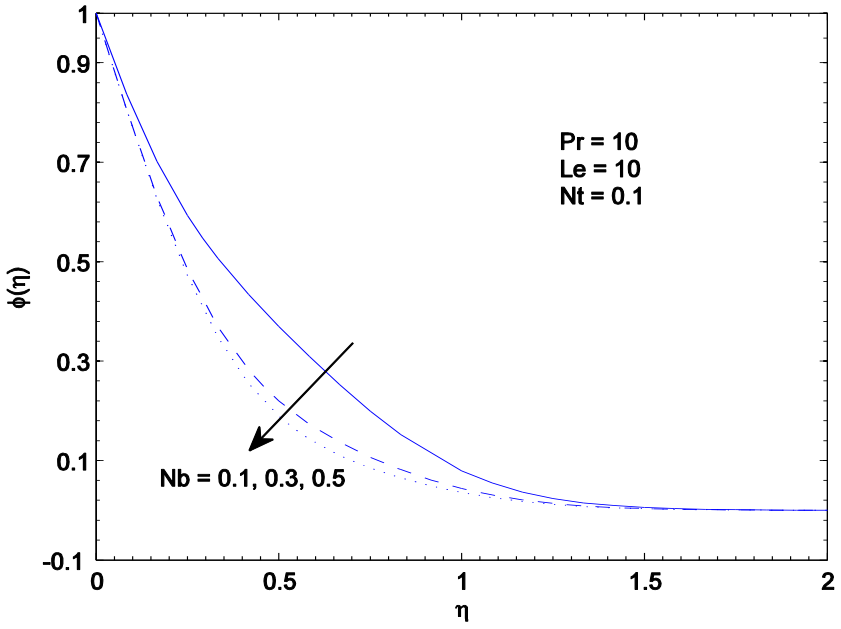

Fig. 3.4: Influence of Nb on nanoparticle volume fraction.

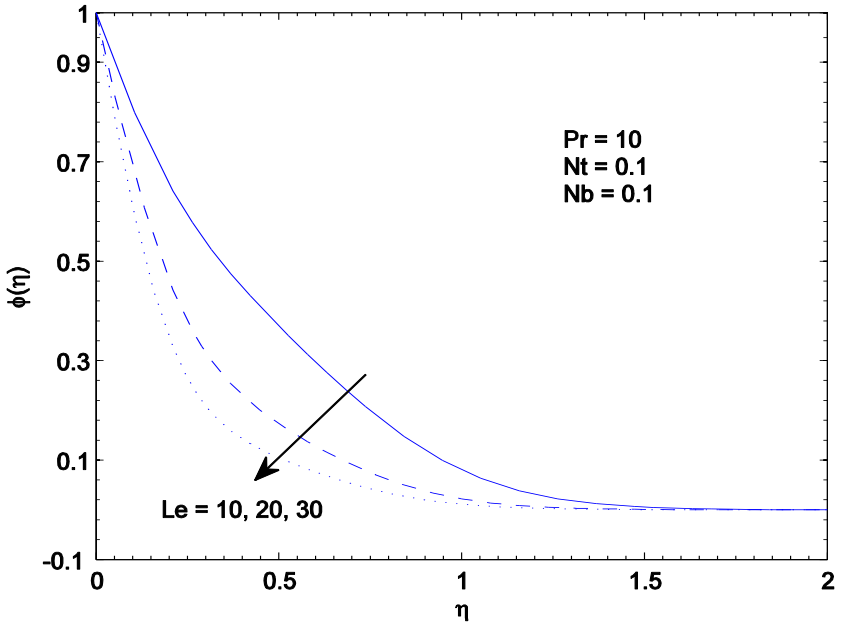

Fig. 3.5: Influence of Le number on nanoparticle volume fraction.

(a)

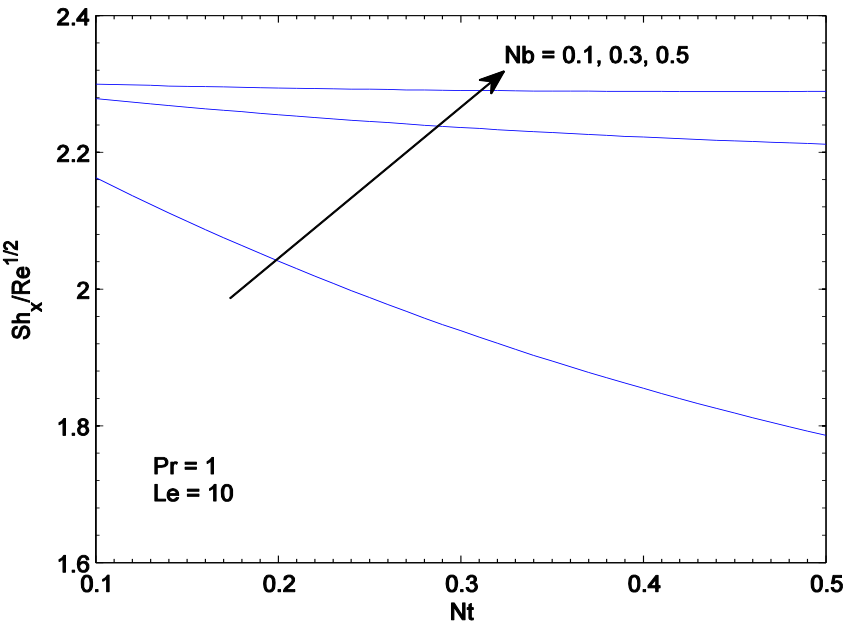

(b)

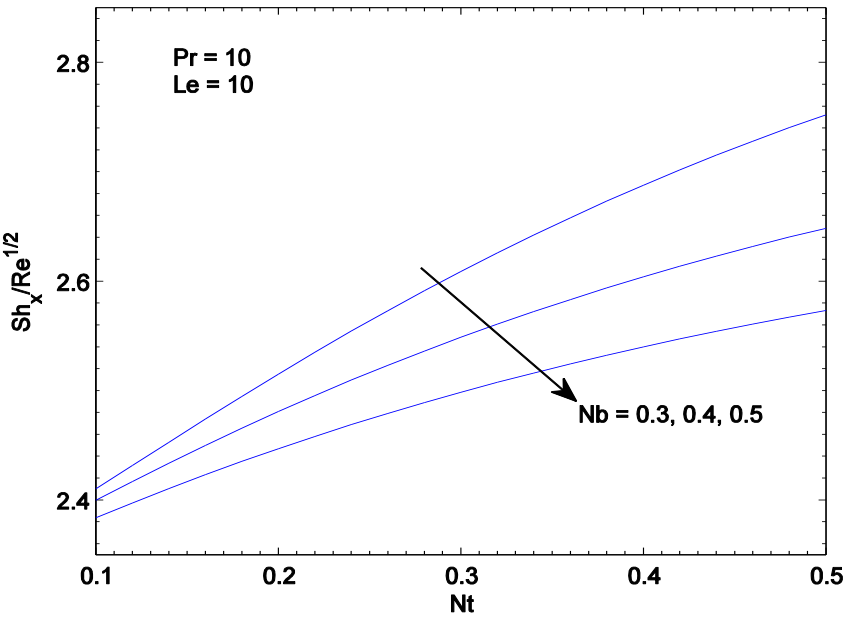

Fig. 3.6: Influence of Nb and Pr on dimensionless mass transfer rates.

(a)

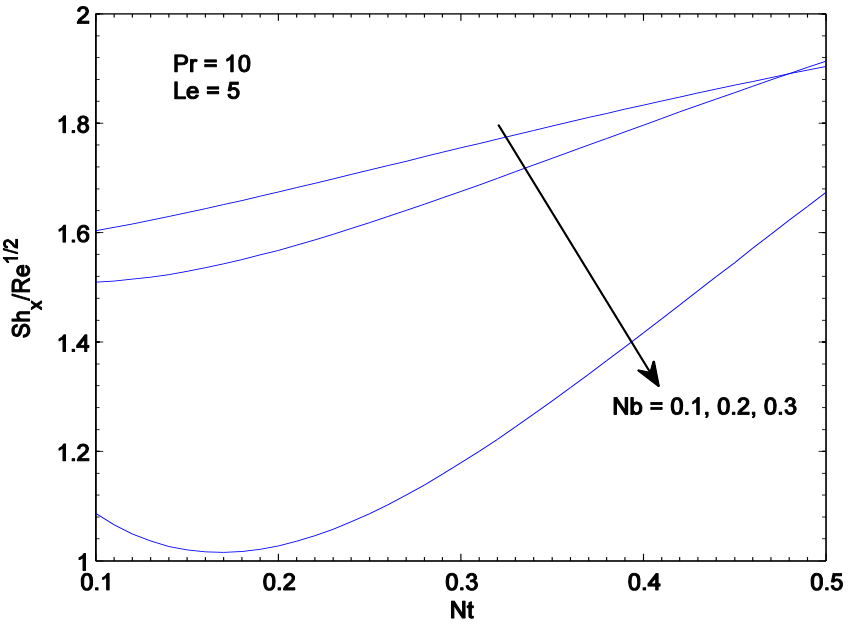

(b)

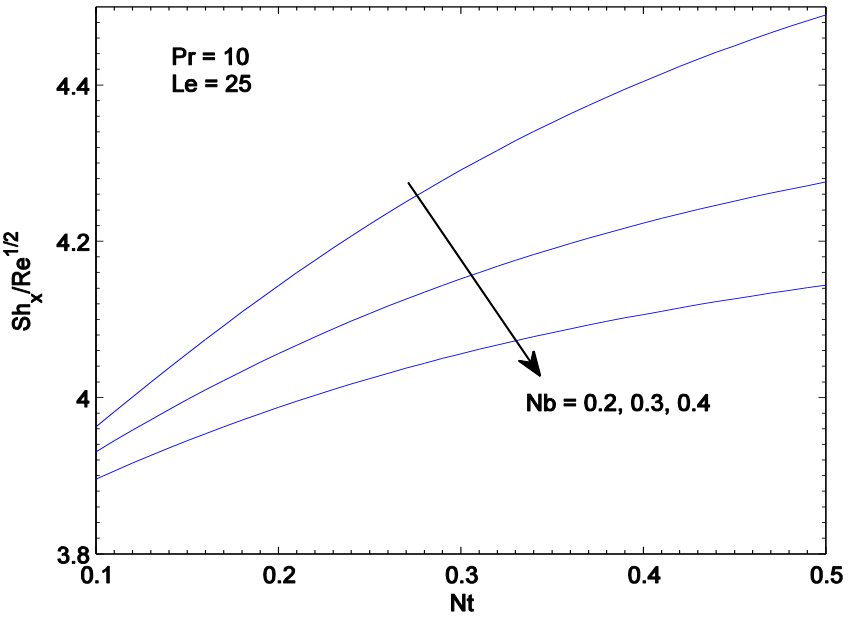

Fig. 3.7: Influence of *Nb* and *Le* on dimensionless mass transfer rates.

Chapter 4

MHD stagnation-point flow of power-law nanofluid towards a stretching sheet

This chapter is organized as follows.
Section 4.1 gives the introduction. Section 4.2 involves mathematical formulation of the problem. Numerical results in the form of graphs and tables are discussed in Section 4.3.

4.1 Introduction

In this chapter the two-dimensional stagnation-point flow of an electrically conducting non-Newtonian nanofluid obeying power-law model [48] is investigated in the presence of Lorentz force. The power-law model can adequately describe the shear thinning/thickening behaviors in non-Newtonian fluids at low and high shear rates (see Bird [48]). It has received tremendous fame in the research community due to its simplicity. The transport equations are formulated through Buongiorno's model that takes into consideration the Brownian motion and thermophoretic diffusion of nanoparticles. The dimensionless mathematical problems are numerically solved by a shooting method for both integer and non-integer values of power-law index(n). The results are shown both graphically and in tabular form for different parametric values and discussed in detail.

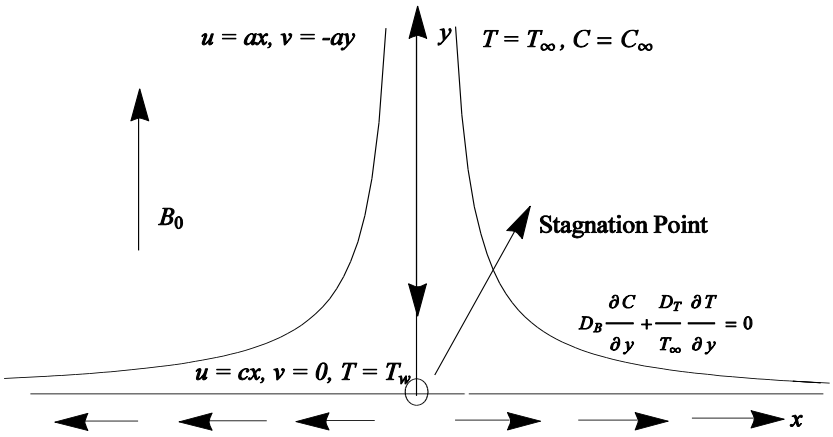

Fig. 4.1: Physical sketch of the problem and coordinate system.

4.2 Basic equations

Let us choose the Cartesian coordinate system as shown in Fig. 4.1. We consider a non-Newtonian flow initiated due to stretching of a plane horizontal surface. The non-Newtonian fluid obeys the well known Ostwalt-de-Waele power-law model [48]. Let $U_w = cx$ be the velocity of the stretching sheet and $U_\infty = ax$ is the velocity outside the boundary layer, where $a, c > 0$ are constants. The sheet is maintained at constant temperature T_w. Whereas mass flux of nanoparticles at the sheet is assumed to be zero and particle fraction value adjusts there accordingly. T_∞ and C_∞ denote the ambient values of temperature and nanoparticle volume fraction respectively. The $x-$ axis is taken along the sheet while $y-$ axis normal to it. A uniform magnetic field of strength B_0 is applied perpendicular to the flow.

The boundary layer equations governing the conservation of mass, linear momentum, energy and nanoparticles are as under (see Mahapatra et al. [25] and Khan and Pop [33] for details):

$$\frac{\partial u}{\partial x} + \frac{\partial v}{\partial y} = 0, \tag{4.2.1}$$

$$u\frac{\partial u}{\partial x} + v\frac{\partial u}{\partial y} = U\frac{dU}{dx} + \frac{1}{\rho}\frac{\partial \tau_{xy}}{\partial y} - \frac{\sigma {B_0}^2}{\rho}(u - U), \tag{4.2.2}$$

in the present problem we have $\partial u/\partial y < 0$ when $a/c < 1$ and $\partial u/\partial y > 0$ when $a/c > 1$. Now re-writing Eq. (4.2.2) after invoking the values of τ_{xy} for these two cases as under (see Mahapatra et al. [25]):

When $a/c < 1$,

$$u\frac{\partial u}{\partial x} + v\frac{\partial u}{\partial y} = U\frac{dU}{dx} - \frac{K}{\rho}\frac{\partial}{\partial y}\left(-\frac{\partial u}{\partial y}\right)^n - \frac{\sigma {B_0}^2}{\rho}(u - U), \tag{4.2.3}$$

and when $a/c > 1$,

$$u\frac{\partial u}{\partial x} + v\frac{\partial u}{\partial y} = U\frac{dU}{dx} + \frac{K}{\rho}\frac{\partial}{\partial y}\left(\frac{\partial u}{\partial y}\right)^n - \frac{\sigma {B_0}^2}{\rho}(u - U), \tag{4.2.4}$$

and the thermal energy and nanoparticle concentration equations are as follows (see Khan and Pop [33])

$$u\frac{\partial T}{\partial x} + v\frac{\partial T}{\partial y} = \alpha\frac{\partial^2 T}{\partial y^2} + \tau\left[D_B\frac{\partial C}{\partial y}\frac{\partial T}{\partial y} + \frac{D_T}{T_\infty}\left(\frac{\partial T}{\partial y}\right)^2\right], \tag{4.2.5}$$

$$u\frac{\partial C}{\partial x} + v\frac{\partial C}{\partial y} = D_B\frac{\partial^2 C}{\partial y^2} + \frac{D_T}{T_\infty}\frac{\partial^2 T}{\partial y^2}, \tag{4.2.6}$$

In the above equations u and v are the velocity components along the $x-$ and $y-$ directions respectively, T is the fluid's temperature, C is the local nanoparticle volume fraction, K is the consistency index, n is the flow behavior index, D_B is the Brownian diffusion coefficient, D_T is the thermophoretic diffusion coefficient and $\tau = (\rho c)_p/(\rho c)_f$ is the ratio of effective heat capacity of the nanoparticle material to the effective heat capacity of the base fluid. The relevant boundary conditions in the present problem are

$$\begin{gathered} u = U_w(x) = cx, v = 0,\ \ T = T_w,\ \ \ D_B\frac{\partial C}{\partial y} + \frac{D_T}{T_\infty}\frac{\partial T}{\partial y} = 0 \text{ at } y = 0, \\ u = U(x) = ax,\ \ v = -ay,\ \ \ T \to T_\infty,\ \ C \to C_\infty \text{ as } y \to \infty. \end{gathered} \tag{4.2.7}$$

We introduce the following variables

$$\psi = \left(\frac{K/\rho}{c^{1-2n}}\right)^{1/(n+1)} x^{2n/(n+1)} f(\eta),\ \ \eta = y\left(\frac{c^{2-n}}{K/\rho}\right)^{1/(n+1)} x^{(1-n)/(1+n)},$$

$$\theta(\eta) = \frac{T - T_\infty}{T_w - T_\infty},\ \ \phi(\eta) = \frac{C}{C_\infty}, \tag{4.2.8}$$

in which ψ is the stream function. Using Eq. (4.2.8), the governing equations (4.2.3) – (4.2.6) become,

$$n[sgn(\lambda - 1)f'']^{n-1} f''' + \left(\frac{2n}{n+1}\right) ff'' - f'^2 - Mf' + M\lambda + \lambda^2 = 0, \tag{4.2.9}$$

$$\theta'' + \Pr\left(\frac{2n}{n+1}\right) f\theta' + PrNb\theta'\phi' + PrNt\theta'^2 = 0, \tag{4.2.10}$$

$$\phi'' + \left(\frac{2n}{n+1}\right) + Scf\phi' + \frac{Nt}{Nb}\theta'' = 0, \tag{4.2.11}$$

and the boundary conditions (4.2.7) become

$$f(0) = 0, \qquad f'(0) = 1, \qquad \theta(0) = 1, \qquad \phi'(0) + \frac{Nt}{Nb}\theta'(0) = 0,$$

$$f'(\infty) = \lambda, \qquad \theta(\infty) = 0, \qquad \phi(\infty) = 0, \tag{4.2.12}$$

where sgn $(.)$ is the "sign" function, M is the magnetic parameter, Pr is the modified Prandtl number, Sc is the modified Schmidt number, Nb is the Brownian motion parameter and Nt is the thermophoresis parameter. These are defined as

$$M = \frac{\sigma {B_0}^2}{\rho c}, Pr = \frac{(K/\rho)^{\left(\frac{2}{n+1}\right)} x^{-2\left(\frac{1-n}{1+n}\right)}}{\alpha c^{3\left(\frac{1-n}{1+n}\right)}}, Sc = \frac{(K/\rho)^{\left(\frac{2}{n+1}\right)} x^{-2\left(\frac{1-n}{1+n}\right)}}{D_B c^{3\left(\frac{1-n}{1+n}\right)}},$$

$$Nb = \frac{\tau D_B C_\infty}{\alpha}, Nt = \frac{\tau D_T (T_w - T_\infty)}{\alpha T_\infty}. \tag{4.2.13}$$

It should be noted that since $x-$coordinate could not be eliminated from the momentum equation, the local similarity solutions of above equations are possible which allows us to explore the behaviors of parameters at a fixed location above the

sheet. Using the dimensionless variables (4.2.8) the skin friction coefficient $C_f = \tau_{yx}\big|_{y=0}/(1/2)\rho(cx)^2$ can be expressed as under:

$$Re_x{}^{1/(1+n)}C_f = 2[sgn(\lambda-1)f''(0)]^n, \tag{4.2.14}$$

Where $Re_x = (cx)^{2-n}x^n/(K/\rho)$ is the local Reynolds number. Further the local Nusselt number $Nu_x = -x\left(\frac{\partial T}{\partial y}\right)_{y=0}/k(T_w - T_\infty)$ takes the following form $Re_x{}^{-1/(1+n)}Nu_x = -\theta'(0) = Nur$. It is worth pointing here that local Sherwood number which is the dimensionless mass flux is identically zero.

4.2.1 Numerical method

The transformed momentum Eqs. (4.2.9)-(4.2.11) subject to the boundary conditions are solved numerically for different values of λ, magnetic parameter M and the power-law index n. First, Eq. (4.2.9)-(4.2.11) can be written as a system of three first-order differential equations, which are solved by standard fourth-order Runge-Kutta integration technique. Let $x_1 = \eta,\ x_2 = f,\ x_3 = f',\ x_4 = f'',\ x_5 = \theta,\ x_6 = \theta',\ x_7 = \phi,\ x_8 = \phi'$. We obtain

$$\begin{pmatrix} x_1' \\ x_2' \\ x_3' \\ x_4' \\ x_5' \\ x_6' \\ x_7' \\ x_8' \end{pmatrix} = \begin{pmatrix} 1 \\ x_3 \\ x_4 \\ \dfrac{-\left(\frac{2n}{n+1}\right)x_2x_4 + x_3{}^2 + Mx_3 - M\lambda - \lambda^2}{n[sgn(\lambda-1)x_4]^{n-1}} \\ x_6 \\ -\left(\dfrac{2n}{n+1}\right)Prx_2x_6 + Nbx_8x_6 + Ntx_6{}^2 \\ x_8 \\ -\left(\dfrac{2n}{n+1}\right)Lex_2x_8 - \dfrac{Nt}{Nb}x_6{}' \end{pmatrix},$$

and the corresponding initial conditions are

$$\begin{pmatrix} x_1(0) \\ x_2(0) \\ x_3(0) \\ x_4(0) \\ x_5(0) \\ x_6(0) \\ x_7(0) \\ x_8(0) \end{pmatrix} = \begin{pmatrix} 0 \\ 0 \\ 1 \\ u_1 \\ 1 \\ u_2 \\ u_3 \\ -\frac{Nt}{Nb}u_2 \end{pmatrix}.$$

The above nonlinear ODEs along with initial conditions are solved by standard fourth-order Runge-Kutta integration technique. Suitable values of the unknown initial conditions u_1 , u_2 and u_3 are approximated through Newton's method until the boundary conditions at infinity $f'(\infty)$, $\theta(\infty)$ and $\phi(\infty)$ is satisfied. The computations have been performed by using MATLAB. The maximum value of η to each group of parameters is determined.

4.3 Numerical results and discussions

Table 4.1 provides a sample of our results for reduced Nusselt number $(-\theta'(0))$ with the variation of Pr, Sc and Nt. There is a decrease in $|-\theta'(0)|$ with an increase in N_t. This is because a stronger thermophoretic effect drives the the nanoparticle of high thermal conductivity from the stretching wall to the cold fluid. As a result the thermal boundary layer grows with an increment in Nt. This increase in thermal boundary layer is compensated with the smaller wall slope of temperature function and hence smaller magnitude of reduced Nusselt number. Increasing Prandlt number results in stronger convection compared to pure conduction and hence larger magnitude of reduced Nusselt number. The last four entries of the table reveal that $|-\theta'(0)|$ is a decreasing function of Schmidt number Sc. It is important to mention that influence of Brownian motion parameter D_B on the wall temperature gradient is nearly negligible. This can be seen by using the condition $\phi'(0) = -(Nt/Nb)\theta'(0)$ on the local energy equation (4.2.10) as the wall is approached.

Figs. (4.2)-(4.4) are plotted to perceive the effects of parameters on the thermal boundary layer. Fig. (4.2) indicates that an increase in Prandtl number Pr decreases conduction which results in less penetration depth for temperature θ. The reduction in the thermal boundary layer accompanies with larger slope of temperature function

near the wall. Further an increase in power-law index n corresponds to a decrease in temperature and thermal boundary layer thickness for any considered value of λ. An increase in ratio λ enhances the intensity of the cold fluid at the ambient towards the hot sheet and thus corresponds to a decrease in the fluid's temperature (see Fig. 4.3). For thermophoretic effect the motion of particles occurs due to the temperature gradient towards a cold surface and away from a hot one. Temperature θ is an increasing function of Nt (see Fig. 4.4). Further the influence of Brownian motion on the thermal boundary layer is negligible. In other words the nanoparticles dissipate energy in the form of heat which causes the thermal boundary layer thickness to increase and ultimately a localized rise in fluid's temperature occurs.

Figs. (4.5)-(4.8) give the influences of parameters on the nanoparticle volume fraction distribution. Fig. (4.5) shows that ϕ is a decreasing function of Sc. Physically an increase in Sc corresponds to less mass diffusivity and hence thinner boundary layer for nanoparticle volume fraction. Fig. (4.6) reveals that influence of n and λon ϕ is similar to that accounted for the temperature θ. It is seen from Fig. (4.7) that ϕ increases with the increasing values of Nt. As the thermophoretic effect strengthens, the hot sheet strongly repels nanoparticle from it which leads to thicker boundary layer for ϕ. However nanoparticle volume fraction decreases when $Nb$is increased (see Fig. 4.8).

Figs. (4.9) and (4.10) plot the reduced Nusselt number Nur against Nt and Pr respectively with the variation in power-law index n. We found that for a fixed value of magnetic parameter, the heat transfer rate at the sheet is bigger in the case of dilatant (shear-thickening) fluids when compared with the psuedoplastic (shear-thinning) fluids.

Table 4.1: Values of reduced Nusselt number $(-\theta'(0))$ with the variation of Pr, Sc and Nt when $Nb = 0.1, n = 0.8, M = 1, \lambda = 0.6$.

Pr	Nt	Sc	$-\theta'(0)$
2	0.1	1	0.95175
4			1.37397
6			1.70126
8			1.97847
10			2.22341
	0.2		2.19153
	0.4		2.12687
	0.6		2.06102
	0.8		1.99398
	1		1.92581
		2	1.62745
		4	1.20511
		6	0.96878
		8	0.82843
		10	0.73679

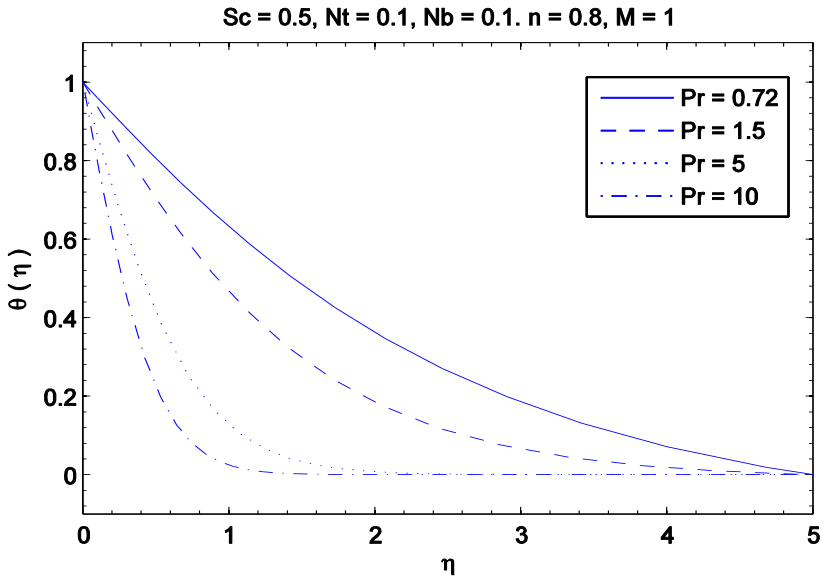

Fig. 4.2: Effect of Pr on temperature θ.

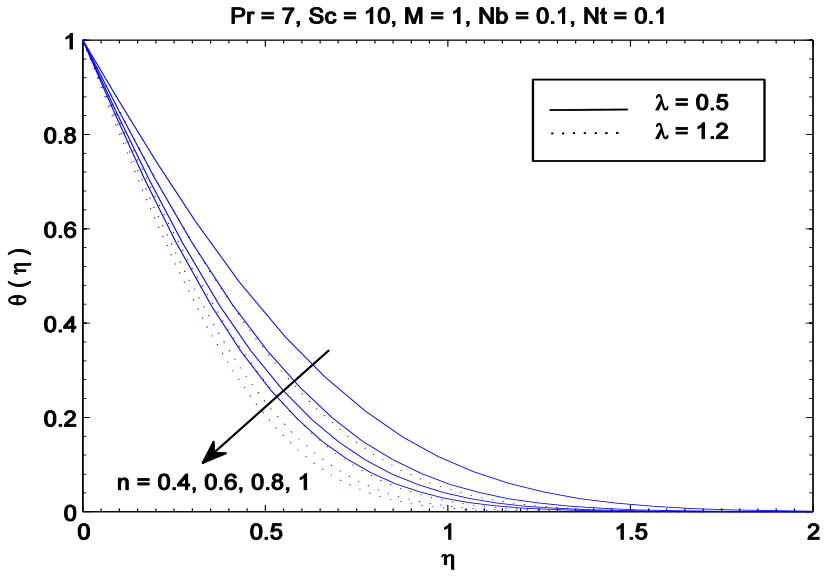

Fig. 4.3: Effect of n and λ on temperature θ.

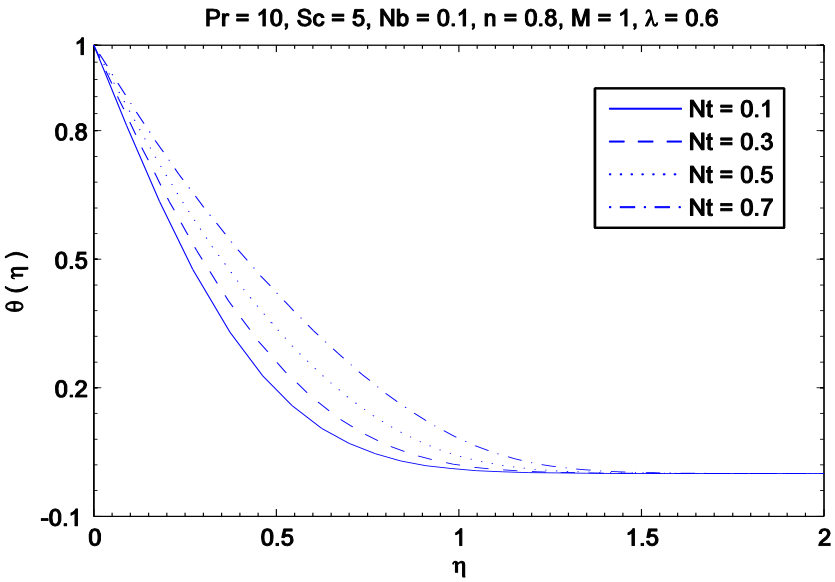

Fig. 4.4: Effect of Nt on temperature θ.

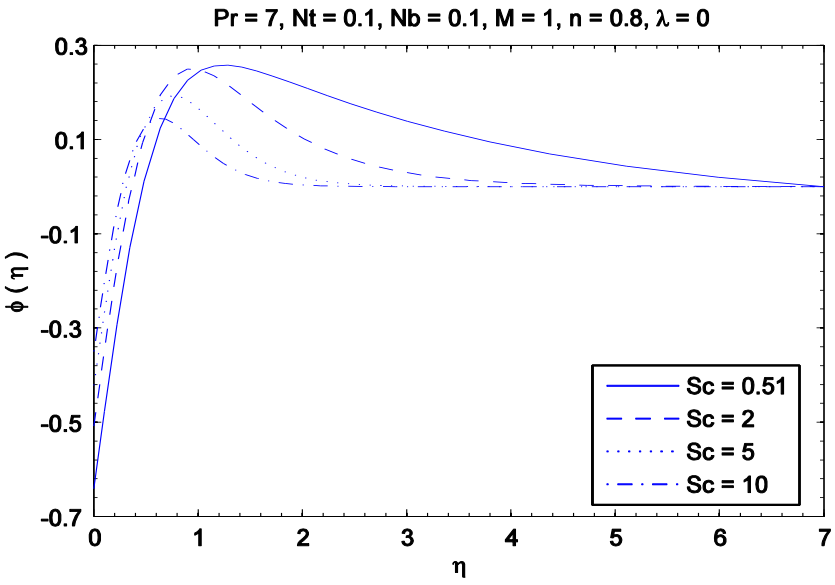

Fig. 4.5: Effect of Sc on nanoparticle volume fraction ϕ.

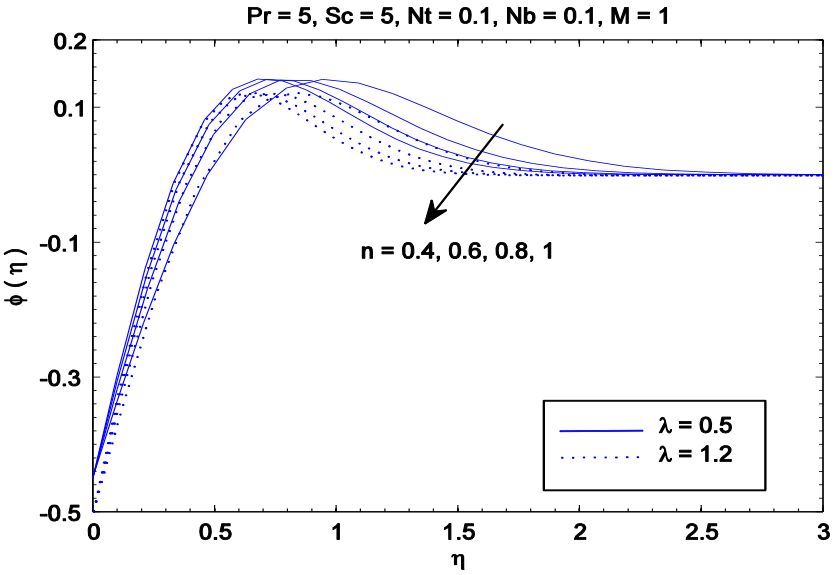

Fig. 4.6: Effect of n and λ on nanoparticle volume fraction ϕ.

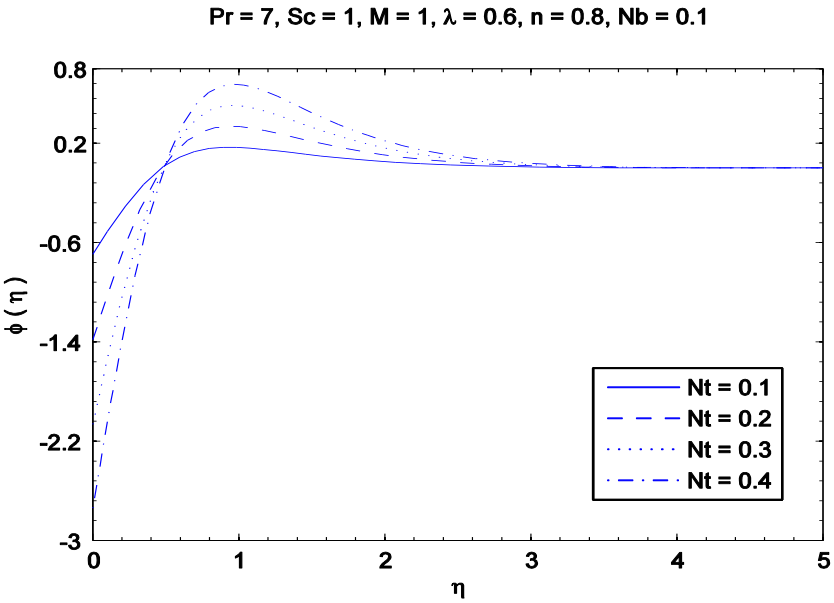

Fig. 4.7: Effect of Nt on nanoparticle volume fraction ϕ.

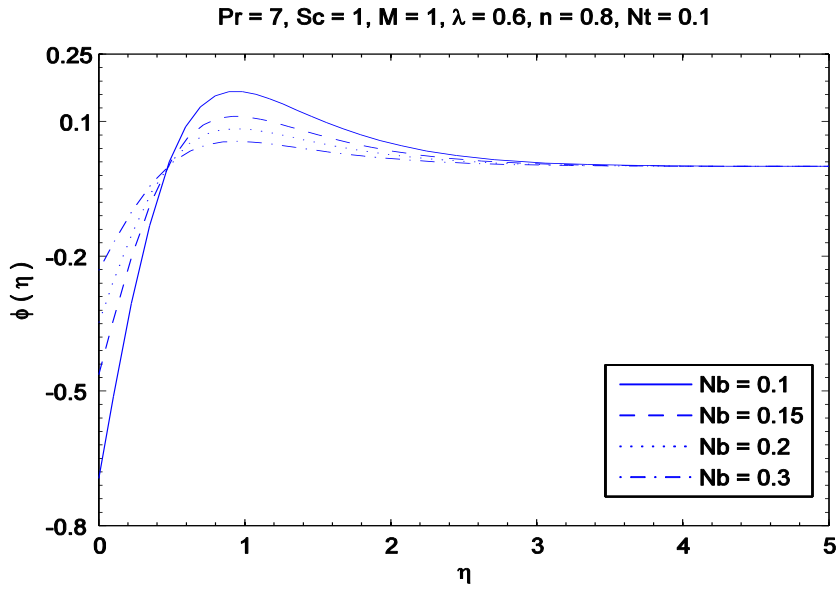

Fig. 4.8: Effect of Nb on nanoparticle volume fraction ϕ.

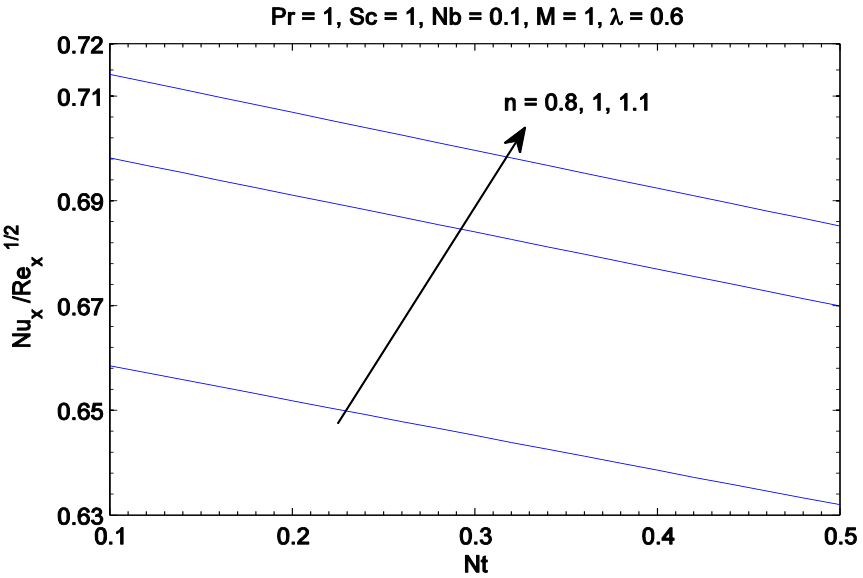

Fig. 4.9: Effect of n on reduced Nusselt number Nur.

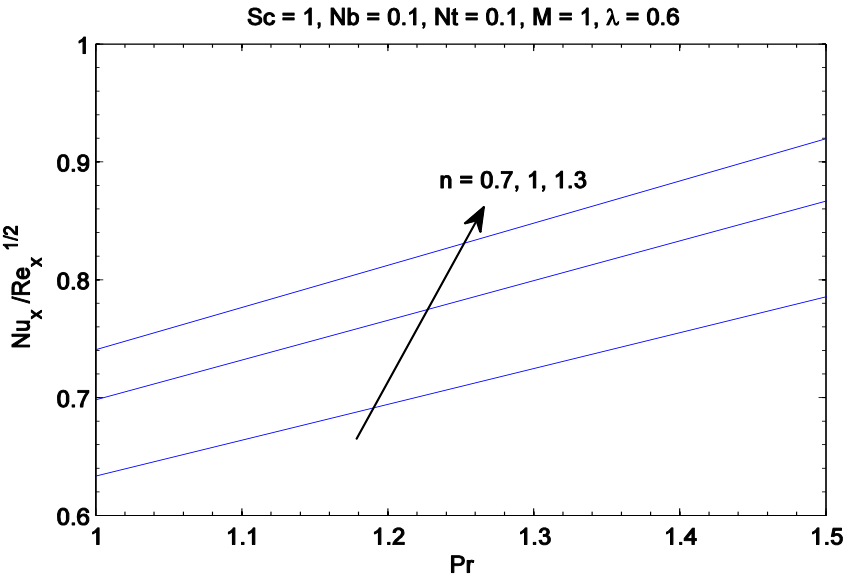

Fig. 4.10: Effect of n on reduced Nusselt number Nur.

Chapter 5

Conclusions

Magnetohydrodynamic (MHD) two-dimensional stagnation-point flow of power-law nanofluid towards an isothermal stretching sheet is studied. The developed mathematical model is solved for the numerical solution by shooting method together with fourth-order Runge-Kutta integration technique. The study reveals that momentum and thermal boundary layers are significantly influenced by varying power-law index n. The key points of this work are outlined below.

1. The velocity distribution increases/decreases with an increase in magnetic field strength when free stream velocity is greater/less than the velocity of the stretching sheet.
2. There is a decrease in wall skin friction $|f''(0)|$ with an increase in power-law index (n) when the free stream velocity is nearly equal to the sheet velocity. However the variation in $|f''(0)|$ is non-monotonic when the velocity ratio largely differs from 1. An outcome that is consistent with the findings of Mahapatra et al. [25].
3. Irrespective of the chosen value of λ, the temperature and nanoparticle volume fraction both decrease by an augmentation in the power-law index (n).
4. Heat transfer rate at the sheet decreases by increasing thermophoresis effect. Further, the thermal boundary layer thickness and heat transfer rate are nearly independent of the Brownian motion parameter.
5. Wall heat transfer rate is larger in dilatants fluids when compared with the pseudoplastic fluids.
6. The solutions in the case of Newtonian fluid (which are not yet reported) can be obtained as special case of present study by substituting $n = 1$.

Bibliography

[1] L. Prandtl, Über Flüssigkeitsbewegung bei sehr kleiner Reibung, Verhandlungen des III Internationalen Mathematiker-Kongresses Heidelberg. (1904) 484–491.

[2] H. Blasius, Grenzschichten in Flüssigkeiten mit kleiner Reibung, Z. Angew. Math. Phys. 56 (1908) 1–37.

[3] L. Howarth, On the solution of the laminar boundary layer equations, Proc. Roy. Soc. of London. 164 (1938) 547-579.

[4] N. Riley, Magnetohydrodynamic free convection, J. Fluid Mech. 18(4) (1964) 577-586.

[5] B. C. Sakiadis, Boundary-layer behavior on continuous solid surfaces: I. Boundary-layer equations for two-dimensional and axisymmetric flow, AIChE J. 7 (1961) 26–28.

[6] L. E. Erickson, L. T. Fan and V. G. Fox, Heat and mass transfer on a moving continuous flat plate with suction or injection, Ind. Eng. Chem. 5 (1966) 19–25.

[7] F. K. Tsou, E. M. Sparrow and R. J. Glodstein, Flow and heat transfer in the boundary layer on a continuous moving surface, Int. J. Heat Mass Transf. 10 (1967) 219–235

[8] L. J. Crane, Flow past a stretching plate, Z. Angew. Math. Phys. 21 (1970) 645–647.

[9] K. B. Pavlov, Magnetohydrodynamic flow of an incompressible viscous fluid caused by the deformation of a plane surface, Magn. Gidrodin. 4 (1974) 146–147.

[10] A. Chakrabarti and A. S. Gupta, Hydromagnetic flow and heat transfer over a stretching sheet, Quart. Appl. Math. 37 (1979) 73-78.

[11] H. I. Andersson, MHD flow of a viscoelastic fluid past a stretching surface, Acta Mech. 95 (1992) 227–230.

[12] N. Ahmad and A. Mubeen, Boundary layer flow and heat transfer for the stretching plate with suction, Int. Comm. Heat Mass Transf. 22(6) (1995) 895–906.

[13] H. S. Takhar, A. J. Chamkha and G. Nath, Unsteady three-dimensional MHD-boundary-layer flow due to the impulsive motion of a stretching surface, Acta Mech. 146 (2001) 59-71.

[14] T. R. Mahapatra and A. S. Gupta, Heat transfer in stagnation-point flow towards a stretching sheet, Int. J. Heat Mass Transf. 38 (2002) 517-521.

[15] R. Nazar, N. Amin, D. Filip and I. Pop, Unsteady boundary layer flow in the region of the stagnation point on a stretching sheet, Int. J. Eng. Sci. 42 (2004) 1241-1253.

[16] A. Devi and M. Thiyagarajan, Steady nonlinear hydromagnetic flow and heat transfer over a stretching surface of variable temperature, Int. J. Heat Mass Transf. 42 (2006) 671-677.

[17] M. A. A. Mahmoud, Thermal radiation effects on MHD flow of a micropolar fluid over a stretching surface with variable thermal conductivity, Phys. A. 375 (2007) 401-410.

[18] A. Ishak, R. Nazar and I. Pop, Hydromagnetic flow and heat transfer adjacent to a stretching vertical sheet, Int. J. Heat Mass Transf. 44 (2008) 921-927.

[19] V. G. Fox, L. E. Ericksen and L. T. Fan, The laminar boundary layer on a moving continuous flat sheet immersed in a non-Newtonian fluid, AIChE J. 15 (1969) 327-333.

[20] L. K. Martinson and K. B. Pavlov, Magnetohydrodynamics on non-Newtonian fluids, Magn. Gidrodin. 11 (1975) 59–67.

[21] C. K. Chen and M. I. Char, Heat transfer on a continuous stretching surface with suction or blowing, J. Math. Anal. Appl. 135 (1988) 568-580.

[22] H. I. Andersson and B. S. Dandapat, Flow of a power-law fluid over a stretching sheet, Stability Appl. Anal. Continuous Media. 1 (1991) 339–347.

[23] H. I. Andersson, K. H. Bech and B.S. Dandapat, Magnetohydrodynamic flow of a power-law fluid over a stretching sheet, Int. J. Non-linear Mech. 27 (1992) 929–936.

[24] R. Cortell, A note on magnetohydrodynamic flow of a power-law fluid over a stretching sheet, Appl. Math.Comput. 168 (2005) 557-566.

[25] T. R. Mahapatra, S. K. Nandy and A. S. Gupta, Magnetohydrodynamic stagnation-point flow of a power-law fluid towards a stretching surface, Int. J. Non-linear Mech. 44 (2009) 124-129.

[26] M. Kumari, I. Pop and G. Nath, Transient MHD stagnation flow of a non-Newtonian fluid due to impulsive motion from rest, Int. J. Non-Linear Mech. 45 (2010) 463-473.

[27] M. Mustafa, T. Hayat, I. Pop and A. Hendi, Stagnation point flow and heat transfer of Casson fluid towards a stretching sheet, Z. Naturforsch. 67a (2012) 70-76.

[28] A. Mushtaq, M. Mustafa, T. Hayat and A. Alsaedi, Effects of Thermal radiation effects on the stagnation-point flow of upper-convected Maxwell (UCM) fluid over a stretching sheet, J. Aerosp. Eng. (ASCE). 0000361 (2013) 1943-5525.

[29] S. U. S. Choi, Enhancing thermal conductivity of fluids with nanoparticles, in: Developments and Applications of Non-Newtonian Flows, FED. 231/MD-66 (1995) 99-105.

[30] J. Buongiorno and L. W. Hu, Nanofluid heat transfer enhancement for nuclear reactor application, MNHMT. DOI: 10.1115/MNHMT2009-18062 (2009).

[31] S. Kakaç and A. Pramuanjaroenkij, Review of convective heat transfer enhancement with nanofluids, Int. J. Heat Mass Transf. 52 (2009) 3187–3196.

[32] A. V. Kuznetsov and D. A. Nield, Natural convective boundary-layer flow of a nanofluid past a vertical plate, Int. J. Thermal Sci. 49 (2010) 243-247.

[33] W. A. Khan and I. Pop, Boundary-layer flow of a nanofluid past a stretching sheet, Int. J. Heat Mass Transf. 53 (2010) 2470-2483.

[34] M. Mustafa, T. Hayat, I. Pop, S. Asghar and S. Obaidat, Stagnation point-flow of a nanofluid towards a stretching sheet, Int. J. Heat Mass Transf. 54 (2011) 25-26.

[35] P. Rana and R. Bhargava, Flow and heat transfer of a nanofluid over a nonlinearly stretching sheet: A numerical study, Commun. Nonlinear Sci. Numer. Simul. 17 (2012) 212-226.

[36] T. G. Motsumi and O. D. Makinde, Effects of thermal radiation and viscous dissipation on boundary layer flow of nanofluid over permeable moving flat plate, Phys. Scr. 86 (2012) 045003.

[37] F. M. Hady, F. S. Ibrahim, S. M. A. Gaied and M. R. Eid, Radiation effect on viscous flow of a nanofluid and heat transfer over a nonlinearly stretching sheet, Nanoscale Res. Lett. 7 (2012).

[38] N. A. A. Mat, N. M. Arifin, R. Nazar and F. Ismail, Radiation effect on Marangoni convection boundary layer flow of a nanofluid. Math Sci. 21 (2012).

[39] S. Nadeem, R. U. Haq, Z. H. Khan, Numerical solution of non-Newtonian flow over a stretching sheet, Appl. Nanosci. DOI: 10.1007/s13204-013-0235-8 (2013).

[40] S. Nadeem, R. U. Haq, N. S. Akbar, C. Lee and Z. H. Khan, Numerical study of boundary layer flow and heat transfer of Oldroyd-B nanofluid towards a stretching sheet, PLoS ONE. DOI: 10.1371/journal.pone.0069811 (2013).

[41] M. Mustafa, T. Hayat and S. Obaidat, Boundary layer flow of a nanofluid over an exponentially stretching sheet with convective boundary conditions, Int. J. Num. Meth. Heat & Fluid Flow. 23 (2013) 945-959.

[42] M. Mustafa, M. A. Farooq, T. Hayat and A. Alsaedi, Numerical and series solutions for stagnation-point flow of nanofluid over an exponentially stretching sheet, PLOS ONE. DOI: 10.1371/journal.pone.0061859 (2013).

[43] R. Kandasamy, I. Muhamin and R. Mohamad, Thermophoresis and Brownian motion effects on MHD boundary-layer flow of a nanofluid in the presence of thermal stratification due to solar radiation, Int. J. Mech. Sci. 70 (2013) 146–154.

[44] R. B. Mohamad, R. Kandasamy and I. Muhamin, Enhance of heat transfer on unsteady Hiemenz flow of nanofluid over a porous wedge with heat source/sink due to solar energy radiation with variable stream condition, Int. J. Heat Mass Transf. 49 (2013) 1261–1269.

[45] A. Mushtaq, M. Mustafa, T. Hayat and A. Alsaedi, Non-linear radiative heat transfer in the flow of nanofluid due to solar energy: A numerical study, J. Taiwan Inst. Chem. Eng. In Press (2013).

[46] M. Turkyilmazoglu, Unsteady convection flow of some nanofluids past a moving vertical flat plate with heat transfer, J. Heat Transf. DOI: 10.1115/1.4025730 (2013).

[47] M. Turkyilmazoglu, Nanofluid flow and heat transfer due to a rotating disk, Comp. Fluids 94 (2014) 139-146.

[48] R. B. Bird, Useful non-Newtonian models, Ann. Rev. Fluid Mech. 8 (1976)13–34.

Appendix

MATLAB code to solve non-linear ODE

For $a/c < 1$

```
function shooting_method_powerlaw3_new
global XSTART XSTOP Pr Le Nb Nt H M n lamda
XSTART  = 0; XSTOP = 5;
Pr      = 7;
Le      = 1;
Nb      = 0.3;
Nt      = 0.1;
H       = 0.1;            % step size
n       = 0.8;
lamda   = 0.6;
M       = 1;
freq    = 1;              % Frequency of printout.
u = [ -0.7547  -1.8814   -0.8854];
x = XSTART;
u = newtonRaphson2(@residual,u);
[xSol,ySol] = runKut5(@dEqs,x,inCond(u),XSTOP,H);
plot(xSol, ySol(:,6))
hold on
ySol(1, :)
theta=ySol(1,5);
sol=vpa(theta,5);
phy=ySol(1,7);
sol=vpa(phy,6);
axis([0 XSTOP -0.8 0.2])
function F = dEqs(t,y)
global Pr Le Nb Nt n lamda M
F = zeros(1,7);
F(1) = y(2);
F(2) = y(3);
yy1  =(   -((2*n)/(n+1))*y(1)*y(3)   +  y(2)*y(2)  +  M*y(2)  - M*lamda -
lamda^2)/(n*((-y(3)).^(n-1)));
F(3) = yy1;
F(4) = y(5);
yy2  = - Pr*(((2*n)/(n+1))*y(1)*y(5) + Nb*y(7)*y(5) + Nt*y(5)*y(5));
F(5) = yy2;
F(6) = y(7);
yy3  = - Le*((2*n)/(n+1))*y(1)*y(7) - (Nt/Nb)*yy2;
F(7) = yy3;
function y = inCond(u)    % Initial conditions; u(1)
```

```
global Nt Nb
y = [0   1   u(1)   1   u(2)   u(3)   -Nt/Nb*u(2)];
function r = residual(u)
global XSTART XSTOP H lamda
r = zeros(length(u),1);
x = XSTART;
[xSol,ySol] = runKut5(@dEqs,x,inCond(u),XSTOP,H);
lastRow = size(ySol,1);
r(1) = ySol(lastRow,2)- lamda;
r(2) = ySol(lastRow,4);
r(3) = ySol(lastRow,6);
```

For $a/c > 1$

```
function shooting_method_powerlaw3_new
global XSTART XSTOP Pr Le Nb Nt H M n lamda
XSTART  = 0; XSTOP = 1;
Pr      = 7;
Le      = 1;
Nb      = 0.3;
Nt      = 0.1;
H       = 0.1;            % step size
n       = 0.8;
lamda   = 0.6;
M       = 1;
freq    = 1;              % Frequency of printout.
u = [ 1 0 0];
x = XSTART;
u = newtonRaphson2(@residual,u);
[xSol,ySol] = runKut5(@dEqs,x,inCond(u),XSTOP,H);
plot(xSol, ySol(:,6))
hold on
ySol(1, :)
theta=ySol(1,5);
sol=vpa(theta,5);
phy=ySol(1,7);
sol=vpa(phy,6);
axis([0 XSTOP -0.8 0.2])
function F = dEqs(t,y)
global Pr Le Nb Nt n lamda M
F = zeros(1,7);
F(1) = y(2);
F(2) = y(3);
yy1  =(   -((2*n)/(n+1))*y(1)*y(3)   +  y(2)*y(2)  +  M*y(2)  - M*lamda -
lamda^2)/(n*((y(3)).^(n-1)));
F(3) = yy1;
F(4) = y(5);
```

```
yy2  = - Pr*(((2*n)/(n+1))*y(1)*y(5) + Nb*y(7)*y(5) + Nt*y(5)*y(5));
F(5) = yy2;
F(6) = y(7);
yy3  = - Le*((2*n)/(n+1))*y(1)*y(7) - (Nt/Nb)*yy2;
F(7) = yy3;
function y = inCond(u)    % Initial conditions; u(1)
global Nt Nb
y = [0   1   u(1)   1   u(2)   u(3)   -Nt/Nb*u(2)];
function r = residual(u)
global XSTART XSTOP H lamda
r = zeros(length(u),1);
x = XSTART;
[xSol,ySol] = runKut5(@dEqs,x,inCond(u),XSTOP,H);
lastRow = size(ySol,1);
r(1) = ySol(lastRow,2)- lamda;
r(2) = ySol(lastRow,4);
r(3) = ySol(lastRow,6);
```